Submitted for publication

Phase Field Simulation of Anisotropic Grain Coarsening Using a Generalized Dislocation Zone-Based Grain Boundary Model

S. Hao[a,b]
[a]Department of Mechanical Engineering/Department of Materials Science and Engineering
Northwestern University, Evanston IL 60208
[b]ACII-Consulting, Wilmette, IL 60091

Abstract

A multi-dimensional phase field model of anisotropic polycrystalline has been developed based on Ginzburg-Landau(GL) theory and a dislocation representation of grain boundaries. In this model the order parameter refers to the average amplitude of the density of electron gas; and a grain boundary is treated as a generalized dislocation zone, distinguishing from bulk crystal. The system free energy is constructed by Bloch's wave functions in the form of Ginzburg-Landau expansion with the coefficients that are a series of combined functions of order parameter, its gradient, the angles of grain boundary tilt and misorientation; whereby the interfacial "structural factor" has been derived applying Peierls-Nabbaro's dislocation potential. Hence, these coefficents can be determined by either experimental calibration or first principle computation. Two and three dimensional numerical examples of single specie system demonstrate that the developed model is capable to reproduce coarsening process.

Keywords: phase field models, grain growth, dislocations, interface, diffusion-induced grain boundary motion (DIGM), analytical methods

1. INTRODUCTION

1.1 Phase Field Theory

Phase field model has been widely employed as numerical tools to reproduce diffusion-based physical processes associated with the motions of interfaces in heterogeneous system[1-12, 16-18]. For modeling and simulation of the microstructure evolutions during grain solidification and coarsening, it can be considered as a continuum description of the average over randomly atomic motions in a multi-phase polycrystalline system, see the reviews, e.g. [11, 13-15]. In such a system, denoted as the domain Ω, each grain is characterized by its physical state, e.g. the free energy that is the function of an order parameter η_k and state variables such as temperature (T); where η_k is normalized to be unit inside the k^{th} grain but vanishing outside. So the free energy, denoted as F, can be expressed as the following integral over the domain:

$$F = \int_{\Omega} \sum_{k} dV \left[f(\eta_k, T) + \Gamma\left(|\nabla \eta_k|, T \right) \right] \tag{1}$$

where f is a function related to the free energy at each material element in bulk phase; Γ is a function of the gradient of the order parameter so it characterizes the fluctuation at grain boundary.

Hence, for a time-dependent process the evolution of free energy F is a function of the evolution of order parameter and its divergence according to Ginzburg-Laudau formulation [1-3]:

$$\frac{\partial \eta_k}{\partial t} = -\lambda \frac{\partial f(\eta_k, T)}{\partial \eta_k} + \kappa \nabla^2 \eta_k \tag{2}$$

where λ and κ are material's constants. (2) essentially is a degenerated form of the convection-diffusion equation in continuum fluid mechanics without convection.

In recent years, significant progresses can be found in the modeling of solidification process. For binary systems or alloys with more than one components, additional groups of order parameters have been introduced into phase field model [8]. The development of this class of theories, in conjunction with crystalline anisotropy, led to better understanding the kinetics of interfacial motion for dendrite growth of single grain [6, 9, 12, 19-23]. In order to describe the correlation between crystal deformation and solidification, lattice elasticity has been implemented into free energy [22, 24]. Under the time scales between atomic vibration and mesoscopic diffusion, in [22, 25, 26] elastic interactions have been mediated through wave models. As a count part of continuum theory, recently the molecule dynamics-based atomistic analysis [27-30] has received increased attentions, leading to a new avenue to explore interfacial properties [6, 31-33]. Based on Ginzburg-Landau formulation, the liquid-solid interface models for various crystal structures have been studied in [32, 37, 38]. Beyond solidification and coarsening, phase field models have also been successfully applied for the simulations of martensitic transformation, dislocations evolution, plastic deformation, crack growth and many others[39-42]. Considering polycrystalline is a complex system[43], methodologies of numerical schemes in computational materials and mechanics can be found, e.g. in [44-55,77].

The process of grain coarsening is another primary focus of phase field methods[11, 56-58]. For an anisotropic grain, a formulation of the free energy density including crystallographic orientation is proposed in [10, 11, 59]:

$$F = \int dV \left[f(\eta, T) + \frac{\alpha^2}{2} \Gamma^2 \left(|\nabla \eta|, \theta - \psi \right) + sg(\eta) |\nabla \theta| + \frac{\varepsilon^2}{2} h(\eta) |\nabla \theta|^2 \right] \tag{3}$$

where ψ is the angle between grain boundary surface (originally defined as solid-liquid interface) normal and a specified direction, e.g. the x-coordinate in Cartesian system; θ is a specified orientation of crystalline so $\nabla\theta$ is the "misfit" angle at grain boundary between grains; Γ, g, and h are functions of η and θ, respectively; α, s, and ε are coefficients to be determined. The equation (3) is termed "WKC model" in this paper

since it first systemically presents the free energy as a function of tilt angle ψ, orientation angle θ, and the gradient of θ.

For a polycrystalline with *q* grains that contain *n* species components at constant temperature, a total free energy equation for isotropic system has been introduced in [7, 60, 61]:

$$f = \sum_{i=1}^{q}\left[-\frac{\alpha}{2}\eta_i^2 + \frac{\beta}{4}\eta_i^4\right] + \gamma\sum_{i=1}^{q}\sum_{j\neq i}^{q}\eta_i^2\eta_j^2\,; \qquad \Gamma = \frac{\kappa}{2}\sum_{i=1}^{q}(\nabla\eta_i)^2 \tag{4}$$

where α, β are constants. In recent years, various phase field models have been developed with different expressions of the free energy field, see the reviews, e.g. [11, 13-15].

However, in the modeling and simulation of coarsening process in anisotropic polycrystalline system, challenge remains in obtaining precise formulation of free energy and associated efficient numerical procedure without presumed parameters. Based on the fundamental researches reviewed previously, this study develops an anisotropic phase field model of polycrystalline coarsening, whereby grain boundary is modeled as a general dislocation zone while the correlated scaling coefficients in the model are calibrated by crystallographic-based analysis and associated quantum mechanical computation. Hence, the derived formulation has closed form without arbitrary fitting coefficient. Numerical examples in two and three-dimensional cases have been performed to verify the theoretical model developed. For simplification, only the cubic lattice system is taken into account.

1.2 Notations

Standard notation is used throughout. Boldface symbol denote tensor, the order of which is indicated by the context. Plain symbols denote scalars or a component of a tensor when a subscript is attached. Repeated indices are summed. For example, in three-dimensional Cartesian system the three unit coordinate vectors are $\{\mathbf{e}_1, \mathbf{e}_2, \mathbf{e}_3\}$. So a vector ***t***:

$$\boldsymbol{t} = [t_i] = t_1\boldsymbol{e}_1 + t_2\boldsymbol{e}_2 + t_3\boldsymbol{e}_3 \quad \text{or} \quad \boldsymbol{t} = t_i\boldsymbol{e}_i\,, \quad i = 1,2 \ \ (2D) \ \ \text{or} \ \ i = 1,2,3 \ \ (3D)$$

For two order tensors **a** and **b**: $\boldsymbol{a} = [a_{ij}] = a_{ij}\boldsymbol{e}_i\boldsymbol{e}_j$, $\boldsymbol{b} = [b_{ij}] = b_{ij}\boldsymbol{e}_i\boldsymbol{e}_j$; and

$$\boldsymbol{a}\cdot\boldsymbol{b} = [a_{ik}b_{kj}] = a_{ik}b_{lj}\boldsymbol{e}_i\boldsymbol{e}_k\cdot\boldsymbol{e}_l\boldsymbol{e}_j = a_{ik}b_{lj}\boldsymbol{e}_i\boldsymbol{e}_j\delta_{kl} = a_{ik}b_{kj}\boldsymbol{e}_i\boldsymbol{e}_j\,,$$
$$\boldsymbol{ab} = [a_{ij}b_{kl}] = a_{ij}b_{kl}\boldsymbol{e}_i\boldsymbol{e}_j\boldsymbol{e}_k\boldsymbol{e}_l$$
$$\boldsymbol{a}:\boldsymbol{b} = \boldsymbol{a}\cdot\cdot\boldsymbol{b} = [a_{ij}b_{ij}] = a_{ij}b_{ij}$$

2 Proposed Model

2.1 Grain Boundary and Generalized Dislocations Zone

Coarsening essentially is the motions of grain boundaries determined by alloy's chemical composition, thermodynamic environment, and imposed force and displacement conditions [1,2, 76, 49, 50, 66, 67]. Grain boundaries form a network of the interfaces between crystals, representing discontinuities of the periodic atomic arrays. When an interface distinguishes crystals from two different species, it usually forms a coherent or semi-coherent boundary between matrix and second phase particles, e.g. precipitates and inclusions; when an interface is in-between the crystals of the same specie, it defines a grain boundary. In the following analysis, all of the two aforementioned geometric "discontinuities" are termed "grain boundary". From structural viewpoint, these heterogeneities can be simply classified into the following categories[62]: titled, mis-orientated, misfitted boundaries, and a combination of them with or without segregated impurities (see Fig. 1a-1d).

Since a grain boundary represents a continuous deviation from a long-ranged order of atomic array, which can also be viewed as a "generalized dislocations zone" that includes accumulated dislocations and segragated atoms and empties. Such a "general dislocation zone" is a low-ordered structure, i.e. periodically only along the directions parallel to the interface between grains. Introductions of dislocation theory can be found, e.g. in [63, 64].

An immediate consequence of such a generalized dislocation zone is the reduction of adhesion energy. Let E^{coh} be the atomic coherent energy per unit area of a defect-free crystal and E^{gb} the coherent energy of a grain boundary, then according to Fig. 1 this reduction can be approximately expressed as a linear combination below:

$$E^{gb} = E^{coh} - \Delta E^{tilt} - \Delta E^{misore} - \Delta E^{misfit} - \Delta E^{segregate} \tag{5}$$

where ΔE^{tilt}, ΔE^{misore}, ΔE^{misfit}, and $\Delta E^{segregate}$ are the deductions due to grain boundary tilt, misorientation, misfit, and impurities segregations, respectively. Similarly, when a grain boundary becomes a slip plane (γ plane), the corresponding energy barrier against gliding, denoted as γ_P^{GB}, will also be different from bulk phase:

$$\gamma_P^{GB} = \gamma_P \pm \Delta\gamma^{tilt} - \Delta\gamma^{misore} - \Delta\gamma^{misfit} - \Delta\gamma^{segregate} \tag{6}$$

where γ_P is Peierls' energy barrier in bulk crystal; the rest terms are these the same as that in (5). The reason for the "$\pm$" in the front of $\Delta\gamma^{tilt}$ is that by certain tilt angle the energy barrier against gliding can be higher than bulk phase; e.g. an anti-phase boundary such as a twin. The deduction of adhesion energy from bulk phase to boundary causes the changes of order parameter η_k in equation (1).

When a grain boundary is formed by multiple atomic layers, the total adhesion energy per unit area can be expressed as

$$\int_{w} E^{gb} = E^{gb} \frac{w}{\bar{b}} \tag{7}$$

where w is the width of the grain boundary, $\bar{b}$ is the average of the lattice constants from the species of the both side of the boundary.

The proposed "generalized dislocation zone" model enables to apply the results of plasticity for analyzing grain boundary's motion. According to the historical development of solid mechanics, "plasticity" is a theory that describes the average behavior of dislocations-induced atomistic motion by analogy to fluid dynamic theory. The ideally-perfect plasticity, an extreme case of solid, is also an extreme case of viscous flow. This implies an underlying intrinsic connection between these two classes of phenomena, leading to an avenue to combine well-established dislocation-based plasticity theories, e.g. [65,66,78,79], and phase field model for modeling and simulation of anisotropic grains coarsening.

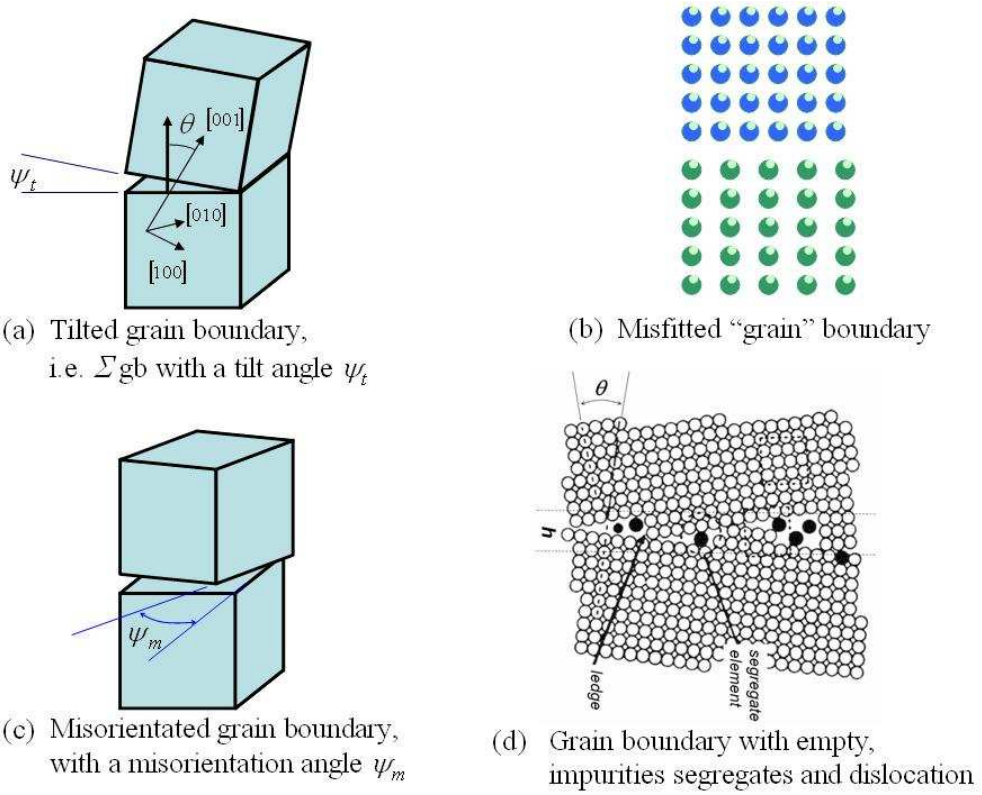

(a) Tilted grain boundary, i.e. Σgb with a tilt angle ψ_t

(b) Misfitted "grain" boundary

(c) Misorientated grain boundary, with a misorientation angle ψ_m

(d) Grain boundary with empty, impurities segregates and dislocation

Fig. 1: Grain boundary heterogeneities

2.2 Geometric Representations of Grain Boundary: Misorientation and Tilt

For simplification this paper focuses on single specie polycrystalline system with cubic crystal structure.

A key-issue in grain boundary analysis is to establish an ambiguity-free geometric representation. A three-step superposition model is introduced for this purpose, which starts with two adjacent grains *A* and *B* with the same lattice orientation, see Fig. 2a. The final position of the grain boundary is obtained by the superposition of the following three virtual motions: (i) an anticlockwise rotation of the grain *B* around [001] to obtain misorientation angle ψ_m, Fig. 2b; (ii) a clockwise rotation ψ_t around the actual position of $\boldsymbol{t}_1^{B^*}$ of *B* to define the tilt, Fig. 2c; (iii) a rotation of the interface surface with normal $\boldsymbol{n_A}$ from $(001)_A$ to its actual position when the angle between $\boldsymbol{n_A}$ and $\boldsymbol{g}_n^{BA^*}$ to be θ_B^n , Figs. 2d, where θ_B^n is the angle with the minimum value among these between $\boldsymbol{n_A}$ and all lattice orientations of grain *B*.

Similarly, the grain boundary representation can also be obtained through fixing *B* while performing the virtual motions to the grain *A*, by which θ_A^n is the angle with the minimum value among these between $\boldsymbol{n_A}$ and all lattice's orientations of the grain *A*.

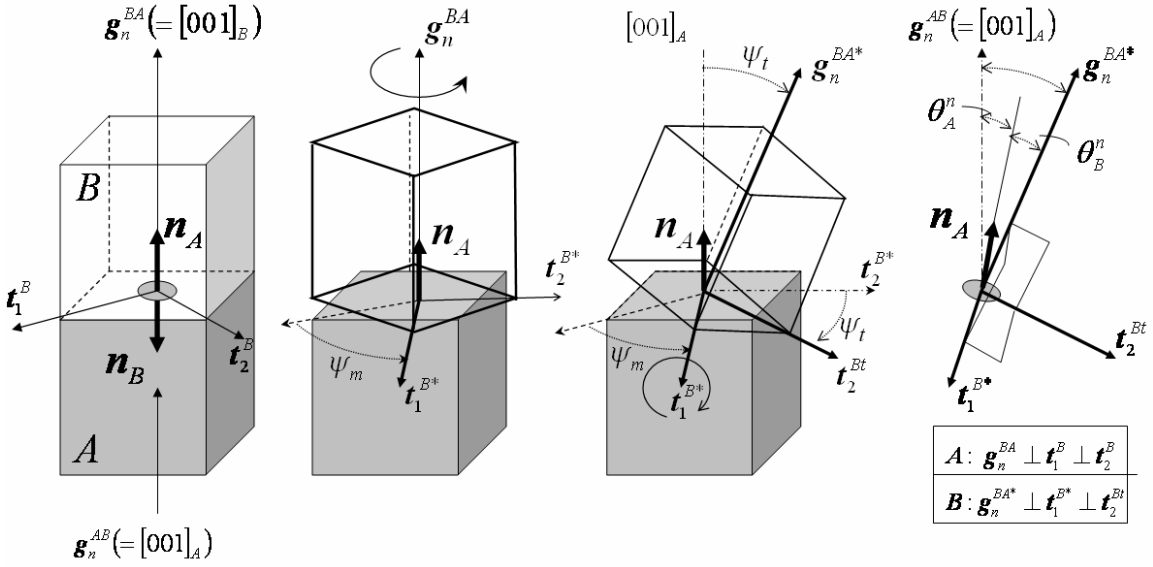

(a) (b) misorientation (c) tilt (d) surface rotation

Fig. 2 A grain boundary with tilt angle ψ_t and misorientation ψ_m can be represented as a superposition of three virtual motions: (a) two grains with coincided crystal orientation initially; (b) an anticlockwise misorientation rotation ψ_m of the grain *B* around $[001]_A$; (c) a clockwise title rotation ψ_t around the vector $\boldsymbol{t}_1^{B^*}$ orthogonal to $[001]_B$; (d) a rotation of grain boundary surface to its actual orientation. Two Cartesian coordinate systems: $\left\{\boldsymbol{t}_1^{B^*}, \boldsymbol{t}_2^{Bt}, \boldsymbol{g}_n^{BA^*}\right\}$ and $\left\{\boldsymbol{t}_1^{B}, \boldsymbol{t}_2^{B}, \boldsymbol{g}_n^{BA}\right\}$ are embedded in grain *B* and *A*, respectively. The $[001]_B$ is chosen to be the lattice vector with the minimum angle to the grain

boundary normal $\boldsymbol{n_A}$. All vectors in (a)-(d) have the same unit length; however, they are plotted with different sizes for easy views.

3. Electron Density-Based Expression of Order Parameter and Ginzburg-Landau Theory

In phase field theories a challenge is to establish the quantitative relationship between the order parameter η_k introduced in (1-3) and the atomic-electronic structure-based energy measurements. In this section the density-functional theory [68, 69] and Ginzburg-Landau's formulation have be applied to derive a governing equation of the anisotropic phase-field. Introduction of Ginsburg-Landau's theory can be found, e.g. in [50].

3.1 Electron density and general dislocation zone

According to density functional theory, the physical state of a material is determined by the core structure of atoms and the statistic distribution of electrons' spin and orbits, which can be described by the density distribution of electrons, denoted as $\rho(\boldsymbol{r})$. The associated energy is the integration of $\rho(\boldsymbol{r})$ over the system. Therefore, this electron density essentially determines the order of the atomic system. For long-range order crystal, e.g. in an infinite large bulk crystal *A,* the electron density can be expressed by the Bloch's theorem [70]

$$\rho^A(\boldsymbol{r}) = \sum_{K^A} \overline{u}_K^A \exp\left(i\boldsymbol{K}^A \cdot \boldsymbol{r}\right) \tag{8}$$

where $\boldsymbol{K^A}$ are the reciprocal-lattice basis vectors in bulk crystal; $\overline{u}_K^A$ are the coefficients and $\boldsymbol{r}$ is position vector; the superscript "*A*" denotes the quantities associated with a grain *A*. The sum in (8) is over all $\boldsymbol{K^A}$ including $\boldsymbol{K}^A = \boldsymbol{0}$.

When the grain *A* is defined within a finite domain Ω_A, this study proposes a Bloch's formulation with order parameter:

$$\rho^A(\boldsymbol{r}) = \sum_{K^A} \overline{u}_K^A(\boldsymbol{r}) exp\left(i\boldsymbol{K}^A \cdot \boldsymbol{r}\right) = \eta^A(\boldsymbol{r})\rho_0\left(\sum_{K^A} u_K^A \, exp\left(i\boldsymbol{K}^A \cdot \boldsymbol{r}\right)\right) \qquad \boldsymbol{r} \in \Omega_A \tag{9}$$

where ρ_0 is a constant; $\eta^A(\boldsymbol{r})$ is the order parameter associated with grain *A*, which actually is a scaling function that is constant inside the grain but varies at its boundary, see Fig. 3; u_K^A are the coefficients and $\overline{u}_K^A = \eta^A \rho_0 u_K^A$.

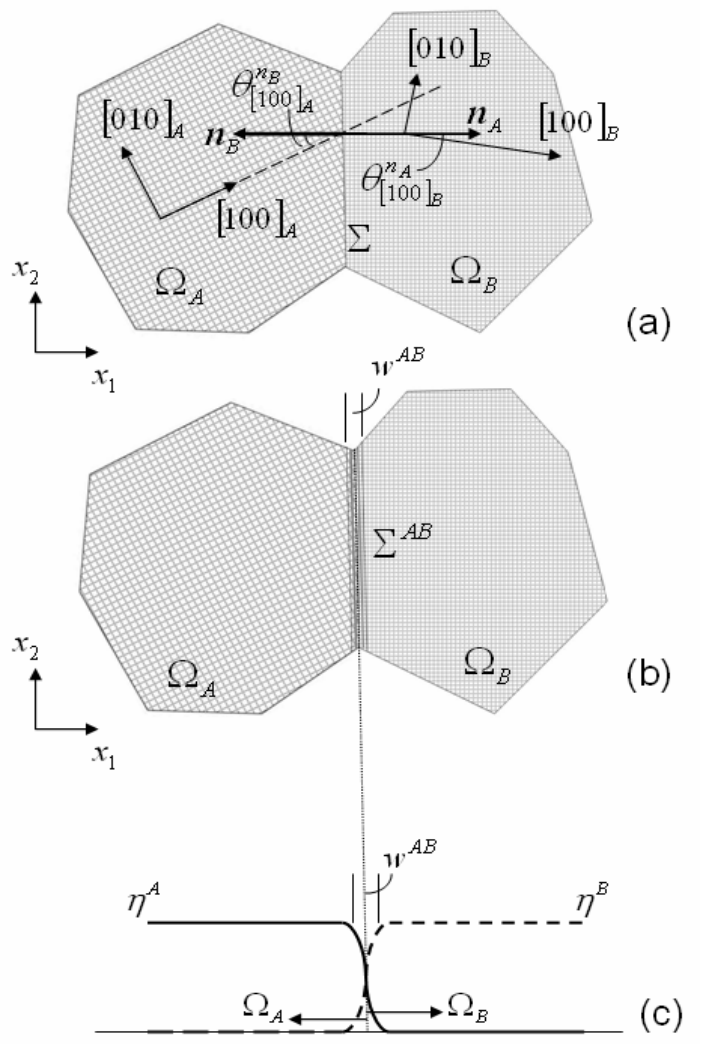

Fig. 3 A bicrystal system with the order parameters η^A and η^B

Considering the bicrystal system illustrated in Fig. 3: $\Omega_{AB} = \Omega_A + \Omega_B$ and $\Omega_A \cap \Omega_B = 0$. For simplification, it is presumed that both *A* and *B* are the same cubic crystals but with different orientations, corresponding to two built-in Cartesian coordinates $\left\{\boldsymbol{t}_1^{B*}, \boldsymbol{t}_2^{Bt}, \boldsymbol{g}_n^{BA*}\right\}$ and $\left\{\boldsymbol{t}_1^{B}, \boldsymbol{t}_2^{B}, \boldsymbol{g}_n^{BA}\right\}$, respectively, as illustrated in Fig.2. In the analysis thereafter a "crystal" refers a "grain" and vice versa. Similarly to (8), for the grain *B* its electron density can also be expressed as:

$$\rho^B(\boldsymbol{r}) = \eta^B(\boldsymbol{r})\rho_0 \sum_{K^B} u_K^B \exp\left(i\boldsymbol{K}^B \cdot \boldsymbol{r}\right) \quad \boldsymbol{r} \in \Omega_B \tag{10}$$

Hence, the reciprocal-lattice basis vector $\boldsymbol{K}^{\boldsymbol{A}}$ defined in grain A can be expressed as $\boldsymbol{K}^{\boldsymbol{B}}$ in the coordinate defined in grain *B* through a two-order rotation tensor $\boldsymbol{Q}^{AB}$:

$$\boldsymbol{K}^A = \boldsymbol{Q}^{AB} \cdot \boldsymbol{K}^B \tag{11}$$

and

$$\boldsymbol{K}^B = \boldsymbol{Q}^{BA} \cdot \boldsymbol{K}^A \qquad \text{where} \qquad \left(\boldsymbol{Q}^{AB}\right)^{-1} = \boldsymbol{Q}^{BA} \tag{12}$$

$\boldsymbol{Q}^{AB}$ is determined by the misorientation and title angles between two adjacent grains; which, therefore, defines the transformation between two Cartesian systems $\left\{\boldsymbol{t}_1^{B*}, \boldsymbol{t}_2^{Bt}, \boldsymbol{g}_n^{BA*}\right\}$ and $\left\{\boldsymbol{t}_1^{B}, \boldsymbol{t}_2^{B}, \boldsymbol{g}_n^{BA}\right\}$ in Figs. 3:

$$\begin{aligned} \boldsymbol{K}^B &= \boldsymbol{Q}^{BA} \cdot \boldsymbol{K}^A \\ &= \left(\boldsymbol{t}_1^{B*} \cdot \boldsymbol{K}^A\right)\boldsymbol{t}_1^{B*} + \left(\boldsymbol{t}_2^{Bt} \cdot \boldsymbol{K}^A\right)\boldsymbol{t}_2^{Bt} + \left(\boldsymbol{g}_n^{BA*} \cdot \boldsymbol{K}^A\right)\boldsymbol{g}_n^{BA*} \end{aligned} \tag{13}$$

3.2 Free Energy and Landau-Ginsburg Expansion

For the bi-crystal system in Fig. 3, according to Ginsburg- Landau's theory, the system free energy can be expressed in the form as [32, 37, 50]:

$$F = F_0 + \Phi_2 + \Phi_3 + \Phi_4 + \ldots \tag{14}$$

where $F_0 = F_0(T)$ is a function only depending upon temperature T; Φ_n are the functions of electron densities $\rho^A(\boldsymbol{r}), \rho^B(\boldsymbol{r})$. When $\boldsymbol{r} \in \Omega_A$:

$$\Phi_n = \sum_{I=1}^{n} \left[\eta^A(\boldsymbol{r})\right]^I \left[\eta^B(\boldsymbol{r})\right]^{n-I} \sum_{\boldsymbol{K}^A, \boldsymbol{K}^B} \left\{ \begin{array}{l} u^A_{\boldsymbol{K}_1^A} \cdots u^A_{\boldsymbol{K}_I^A} u^B_{\boldsymbol{K}_{I+1}^B \cdot \boldsymbol{Q}^{BA}} \cdots u^B_{\boldsymbol{K}_n^B \cdot \boldsymbol{Q}^{BA}} \cdot \\ \exp\left\{ i \left[\sum_{J=1}^{I} \boldsymbol{K}_J^A + \sum_{J=I+1}^{n} \left(\boldsymbol{K}_J^B\right)^T \cdot \boldsymbol{Q}^{BA} \right] \cdot \boldsymbol{r} \right\} \end{array} \right\} \tag{15}$$

where $\sum_{\boldsymbol{K}^A, \boldsymbol{K}^B}$ means the sum of all reciprocal vectors $\boldsymbol{K}_I^A, \boldsymbol{K}_J^B$ in grains A and B; a restriction to (15) is that this summation has to form closed polygons, i.e

$$\sum_{J=1}^{I} \boldsymbol{K}_J^A + \sum_{J=I+1}^{n} \left(\boldsymbol{K}_J^B\right)^T \cdot \boldsymbol{Q}^{BA} = 0 \tag{16a}$$

In this analysis, the following sufficient conditions of (16a) are applied:

$$\sum_{J=1}^{I} \boldsymbol{K}_J^A = 0; \qquad \sum_{J=I+1}^{n} \left(\boldsymbol{K}_J^B\right)^T \cdot \boldsymbol{Q}^{BA} = 0, \tag{16}$$

which ensures the free energy to be invariant when $\boldsymbol{r}$ varies inside a grain or moves from one grain to another, allowing the periodic Block wave function to fit the discontinuity at grain boundary through the order parameter η. Therefore, (15), hence (14), is in fact a

generalized expressions of (1,3-4) including the effects of crystal structure and grain boundary through reciprocal vectors under the restriction (16). More detailed discussion about the Ginsburg- Landau's expansion in periodic crystal can be found, e.g. in [50].

3.3 Functional Taylor's Expansion

Obviously, at grain boundary the electron density (9) or (10) deviates from its original periodic distribution in bulk phase. The corresponding change of free energy should be related to the energy barrier against the atomic motion from long-ranged periodic distribution to "dislocated" heterogeneity zone. As suggested in [68, 69], functional analysis is an effective way to obtain the free energy with the best accuracy. By this methodology a fluctuation from a reference state of the free energy is treated as functional variation that has the maximum gradient along the direction normal to grain boundary. The stationary solution provides the conditions to determine the coefficients in (15). Analogy to the analysis in [35, 36], the functional Taylor's expansion of (14) over a domain Ω is

$$\Delta F = \Delta F_1 + \Delta F_2 + ... \tag{17}$$

where

$$\Delta F_1 = \int_{\Omega} d\boldsymbol{x}^3 \frac{\delta F[\rho]}{\delta \rho(\boldsymbol{r})} \delta\rho(\boldsymbol{r}) \tag{18}$$

$$\Delta F_2 = \frac{1}{2} \int_{\Omega}\int_{\Omega} d\boldsymbol{r}^3 d\tilde{\boldsymbol{r}}^3 \frac{\delta^2 F[\rho]}{\delta\rho(\boldsymbol{r})\delta\rho(\tilde{\boldsymbol{r}})} \delta\rho(\boldsymbol{r})\delta\rho(\tilde{\boldsymbol{r}}) \tag{19}$$

……

where $\rho(\boldsymbol{r})$ can be either $\rho^A(\boldsymbol{r})$ or $\rho^B(\boldsymbol{r})$ or both of them. The functional variation of $\rho(\boldsymbol{r})$ in (9) or (10) can be expressed as a fluctuation from a reference state characterized by $\tilde{\eta}_0(\boldsymbol{r})$:

$$\delta\rho(\boldsymbol{r}) = \delta\eta(\boldsymbol{r})\rho_0 \sum_K u_K \exp(i\boldsymbol{K}\cdot\boldsymbol{r}) = (\eta(\boldsymbol{r}) - \tilde{\eta}_0(\boldsymbol{r}))\rho_0 \sum_K u_K \exp(i\boldsymbol{K}\cdot\boldsymbol{r}) \tag{20}$$

which means, as presumed, at grain boundary the Bloch's wave is scaled by order parameter $\eta(\boldsymbol{r})$.

By choosing the reference state $\tilde{\eta}_0(\boldsymbol{r})$ in (20) be the "zero" state, i.e. $\tilde{\eta}_0(\boldsymbol{r}) = 0$, and omitting the terms with the order of $\boldsymbol{K}$ higher than 4 in (17), after tedious derivation it can be proven that the secondary variation, i.e. (19), can be expressed as [32, 35, 37]:

$$\Delta F_2 \approx \frac{k_B T \rho_0}{2} \sum_{\boldsymbol{K},\tilde{\boldsymbol{K}}} u_{\tilde{\boldsymbol{K}}} u_{\boldsymbol{K}} \delta_{0,K+\tilde{K}} \int_{\Omega} d\boldsymbol{r}^3 \left[\frac{\eta_K(\boldsymbol{r})\eta_{\tilde{K}}(\boldsymbol{r})}{S[\boldsymbol{K}]} + \frac{1}{2} \frac{\partial^2 \hat{C}[\boldsymbol{K}]}{\partial \boldsymbol{K}^2} \frac{\boldsymbol{K}^2}{|\boldsymbol{K}|^2} : (\nabla(\eta_K(\boldsymbol{r})\nabla\eta_{\tilde{K}}(\boldsymbol{r}))) \right] \tag{21}$$

where "∇" is the gradient operator and the structure factor "$S(\boldsymbol{K})$", following the terminology in fluid dynamics, is defined by

$$S(\boldsymbol{K}) = \left[1 - \hat{C}_0[\boldsymbol{K}]\right]^{-1} \tag{22}$$

So $\hat{C}[\boldsymbol{K}]$, the fourier transformation of the "direct correlation function" $C(\rho_0; \boldsymbol{r} - \boldsymbol{r}')$ [35, 36], is the only term to be determined. A brief introduction of the derivation of (21) is given by Appendix I.

By analogy with the theory of plasticity, in (19) the functional variation of the electron density plays the similar role as strain whereas the secondary functional variation in (19), or, alternatively, the "direct correlation function" $C(\rho_0; \boldsymbol{r} - \boldsymbol{r}')$ with the fourier transformation in (21) and (22), is somewhat like a material's stiffness matrix. This analogy will be discussed further in next subsection.

On other hand, the first order variational (18) can be expressed as:

$$\Delta F_1 = \int_{\Omega} d\boldsymbol{r}^3 \frac{\delta F[\rho]}{\delta \rho(\boldsymbol{r})} \delta\rho(\boldsymbol{r}) = 2\Phi_2 + 3\Phi_3 + 4\Phi_4 + ... \tag{23}$$

Applying (16) and dropping the terms with the order of $\boldsymbol{K}$ higher than four:

$$\Delta F_1 \approx 2\Phi_2 + 4\Phi_4 \tag{23a}$$

3.4 Structure Factor and Direct Correlation Function

In fluid dynamic analysis [34-36] the direct correlation function $C(\rho_0; \boldsymbol{r} - \boldsymbol{r}')$ is originally employed to establish the connection between particles based on their positions and the bonding energy in-between, representing "stiffness" against motions of particles in the system. Thus, an approximation has been made in this study is that, in the area near or on the interface surface between two grains, $\hat{C}(\boldsymbol{K})$ can be expressed as a dimensionless Peierls' potential in the form of Bloch's wave function as below [64]

$$\hat{C}(\boldsymbol{K}) = \frac{h_0}{h_p} + \mathrm{Re}\{i \exp[i 2\pi b \boldsymbol{K}]\} \tag{24}$$

where b is Burger's vector; h_p and h_0 are the amplitude of the Peierls' energy barrier and its mean value, respectively; both h_p and h_0 are defined as the energy per unit area; Re(f) denotes the real part of the function f inside the blanket. For simplification one may take, e.g.:

$$h_0 = \frac{h_p}{2} \tag{24a}$$

In (24) $\hat{C}(\boldsymbol{K})$ is the fourier transformation of $C(\rho_0;\boldsymbol{r}-\boldsymbol{r}')$ whereas $\boldsymbol{K}$ is the reciprocal vector corresponding to $\boldsymbol{r}$. In cubic crystals there is no essential difference between coordinates and reciprocal coordinates. The second term of (24) has the same structure as its two-order derivatives (or integrals), which actually is the stiffness against edge-like dislocation. The first term of (24), in conjunction with the constant term in the blanket on the right hand of (22), represents the "stiffness" relevant to the change of "dilatation" energy.

By substituting (24) into (22) and (21), applying (16) and omitting the terms with the power higher than the fourth orders of $\boldsymbol{K}$; then applying (13), the resulted equation, together with (23a), leads to:

$$\Delta F \approx \frac{\rho_0 k_B T}{2}\int F_\eta d\boldsymbol{x}^3 \tag{25}$$

and

$$F_\eta = \left\{ \begin{array}{l} 2\sum\limits_{\Lambda=A,B}\sum\limits_{K^\Lambda} u^\Lambda_{K_\alpha} u^\Lambda_{K_\beta}\delta_{0,K_\alpha+K_\beta}\left(\eta^\Lambda\right)^2 + \\ 4\sum\limits_{\Lambda,\Lambda_1=A,B}\sum\limits_{K^\Lambda} u^\Lambda_{K_\alpha} u^\Lambda_{K_\beta}\sum\limits_{K^{\Lambda_1}} u^{\Lambda_1}_{K_\gamma} u^{\Lambda_1}_{K_\chi}\delta_{0,K_\alpha+K_\beta+K_\gamma+K_\chi}\left(\eta^\Lambda\right)^2\left(\eta^{\Lambda_1}\right)^2 + \\ \sum\limits_{\Lambda=A,B}\sum\limits_{K^\Lambda} u^\Lambda_{K_\alpha} u^\Lambda_{K_\beta}\delta_{0,K_\alpha+K_\beta}\left(a_{\alpha\beta}\left(\eta^\Lambda\right)^2 + b_{\alpha\beta}\left(\cos\theta^\Lambda_\alpha\cos\theta^\Lambda_\beta\left|\nabla\eta^\Lambda\right|^2 + \boldsymbol{K}_\alpha\boldsymbol{K}_\beta : \eta^\Lambda\nabla\nabla\eta^\Lambda\right)\right) \end{array} \right\} \tag{25a}$$

where $u^\Lambda_{K_\alpha}$ are the coefficients in (9) or (10) whereas the superscript Λ (=*A,B*) indicates the grain. The first two rows of (25) are corresponding to the terms in (23a) and the third row to (21); in the latter, after applying (24), the coefficients $a_{\alpha\beta}$, $b_{\alpha\beta}$ yield:

$$a_{\alpha\beta} = 1 - \frac{h_0}{h_p} - \sin\left(2\pi b\left|K_\alpha\right|\right)\sin\left(2\pi b\left|K_\beta\right|\right)$$

$$b_{\alpha\beta} = 2\pi^2 b^2\cos\left(2\pi b\left|K_\alpha\right|\right)\cos\left(2\pi b\left|K_\beta\right|\right)$$

$$\cos\theta^\Lambda_\alpha = \frac{\boldsymbol{K}^\Lambda_\alpha}{\left|\boldsymbol{K}^\Lambda_\alpha\right|}\cdot\frac{\nabla\eta^\Lambda}{\left|\nabla\eta^\Lambda\right|} = \frac{\boldsymbol{K}^\Lambda_\alpha}{\left|\boldsymbol{K}^\Lambda_\alpha\right|}\cdot\boldsymbol{n}_A, \qquad \cos\theta^\Lambda_\beta = \frac{\boldsymbol{K}^\Lambda_\beta}{\left|\boldsymbol{K}^\Lambda_\beta\right|}\cdot\boldsymbol{n}_A$$

Notice that $\nabla\eta^\Lambda$ is parallels to $\boldsymbol{n}_\Lambda$ and

$$\nabla\nabla\eta^\Lambda = \nabla\left(\frac{\nabla\eta^\Lambda}{\left|\nabla\eta^\Lambda\right|}\left|\nabla\eta^\Lambda\right|\right) = \nabla\boldsymbol{n}_\Lambda\left|\nabla\eta^\Lambda\right| + \boldsymbol{n}_\Lambda\nabla\left|\nabla\eta^\Lambda\right|$$

In cubic system

$$\left|\nabla \boldsymbol{n}_{\Lambda}\right| = \left|\nabla \theta\right| \tag{26}$$

where θ is the angle between $\boldsymbol{n}_A$ and a reference direction, e.g, one specified lattice direction, so it can be the tilt angle. Hence, the term $\eta\nabla\nabla\eta$ in (25) represents the effect of variation in tilt angle, in other word, the change of grain boundary curvature. By substituting (26) into (25), one can find that the latter has the similar expression as the free energy (3) obtained in [10, 11, 59] but with $\varepsilon = 0$. We will discuss this point again in next section.

Also, the grain boundary (surface) energy per unit area *A* can be calculated approximately by applying of (25):

$$\gamma = \frac{\Delta F}{A} \approx \frac{\rho_0 k_B T}{2} \int_w F_\eta d\boldsymbol{r} \tag{27}$$

where the one-dimensional integration $d\boldsymbol{r}$ is along the direction perpendicular to grain boundary over the length scale "*w*" that represents the thickness of surface layer.

3.5 Short Range Interaction

Since in this study a grain boundary is viewed as a disordered generalized dislocation zone between two long-range ordered atoms arrays, the short-ranged atomic interaction may dominate its diffusion and mechanical behavior. Hence, in the expansion (25) the part constructed by the reciprocal vectors that span primitive cell (the first Brillouin zone) may provide satisfactory precision for computing the fluctuation of the free energy. This postulation is termed the "approximation of short-range interaction" in this paper. On other hand, by performing a rotate or a translate operation to the Cartesian's coordinate in a crystal, i.e. choosing $\boldsymbol{K}_\alpha, \boldsymbol{K}_\beta$ from different coordinates, the free energy (15) and its fluctuation (25) must be invariant, which leads to the normalization principle suggested by Karma *et al.* (Ref.[31] in [13], also see [32]):

$$\sum_{K^\Lambda} \left\{ u^\Lambda_{K_\alpha} u^\Lambda_{K_\beta} \delta_{0,K_\alpha+K_\beta} \right\} = \sum_{I_K \in K^\Lambda} \frac{u^\Lambda_{2I_K}}{\bar{u}^\Lambda_2}; \qquad u^\Lambda_{2I_K} = \bar{u}^\Lambda_2 \left(u^\Lambda_{K_\alpha} u^\Lambda_{K_\beta} \delta_{0,K_\alpha+K_\beta} \right) \tag{28a}$$

$$\sum_{K^\Lambda} u^\Lambda_{K_\alpha} u^\Lambda_{K_\beta} \sum_{K^{\Lambda_1}} u^{\Lambda_1}_{K_\gamma} u^{\Lambda_1}_{K_\chi} \delta_{0,K_\alpha+K_\beta+K_\gamma+K_\chi} = \sum_{I_K \in K^\Lambda} \frac{u^\Lambda_{4I_K}}{\bar{u}^\Lambda_4}; \qquad u^\Lambda_{4I_K} = u^\Lambda_{2I_K} \sum_{J_K \in K^{\Lambda_1}} \frac{u^{\Lambda_1}_{2J_K}}{\bar{u}^\Lambda_2} \tag{28b}$$

and

$$\bar{u}^\Lambda_2 = \sum_{I_K \in K^\Lambda} u^\Lambda_{2I_K}, \qquad \bar{u}^\Lambda_4 = \sum_{I_K \in K^\Lambda} \sum_{J_K \in K^{\Lambda_1}} \frac{u^\Lambda_{2I_K} u^{\Lambda_1}_{2J_K}}{\bar{u}^\Lambda_2} \tag{28}$$

whereby an natural choice is to let each coefficients on the right hand side of (28a,b) proportional to the projection of the corresponding reciprocal vector onto the outer

normal vector of grain boundary surface. This is because the functional Taylor's expansion (17) describes the fluctuation of free energy; the gradient of this fluctuation is the outer normal vector that defines a grain boundary.

As examples, the BCC and FCC crystals, respectively, are picked to compute the coefficients in the proposed free energy formulation.

3.5.1 BCC Crystal

For BCC crystal, the reciprocal vectors corresponding to the lattice vectors that span its primitive cell form a FCC crystal cell. They belong to the group of vectors $\left\langle \frac{1}{2b},\frac{1}{2b},0 \right\rangle$ that contains the following 6 pairs satisfying (16):

$$\begin{aligned}
&\left[\frac{1}{2b},\frac{1}{2b},0\right] \text{ and } \left[-\frac{1}{2b},-\frac{1}{2b},0\right], \qquad \left[\frac{1}{2b},0,\frac{1}{2b}\right] \text{ and } \left[-\frac{1}{2b},0,-\frac{1}{2b}\right] \\
&\left[0,\frac{1}{2b},\frac{1}{2b}\right] \text{ and } \left[0,-\frac{1}{2b},-\frac{1}{2b}\right], \qquad \left[\frac{1}{2b},-\frac{1}{2b},0\right] \text{ and } \left[-\frac{1}{2b},\frac{1}{2b},0\right] \\
&\left[\frac{1}{2b},0,-\frac{1}{2b}\right] \text{ and } \left[-\frac{1}{2b},0,\frac{1}{2b}\right], \qquad \left[0,\frac{1}{2b},-\frac{1}{2b}\right] \text{ and } \left[0,-\frac{1}{2b},\frac{1}{2b}\right]
\end{aligned} \tag{29}$$

For example, considering the coefficients related to the grain A in Fig. 4, where $\theta^{n_A}_{[a,b,c]_A}$ is the angle between the outer normal vector $\boldsymbol{n}_A$ of the grain boundary and $[a,b,c]$ direction of the crystal A; then the coefficients in (25) or (28a) yield

$$\sum_{K^\Lambda}\left\{u^\Lambda_{K_\alpha}u^\Lambda_{K_\beta}\delta_{0,K_\alpha+K_\beta}\right\}=\sum_{I=1}^{6}\frac{u^\Lambda_{2I}}{\overline{u}^\Lambda_2} \qquad \text{for} \quad \Lambda=A,B \tag{30a}$$

where

$$\begin{aligned}
u^A_{21}&=\left|\cos\left(\theta^{n_A}_{\left[-\frac{1}{2},-\frac{1}{2},0\right]_A}\right)\cos\left(\theta^{n_A}_{\left[\frac{1}{2},\frac{1}{2},0\right]_A}\right)\right|, \quad u^A_{22}=\left|\cos\left(\theta^{n_A}_{\left[-\frac{1}{2},0,-\frac{1}{2}\right]_A}\right)\cos\left(\theta^{n_A}_{\left[\frac{1}{2},0,\frac{1}{2}\right]_A}\right)\right| \\
u^A_{23}&=\left|\cos\left(\theta^{n_A}_{\left[0,-\frac{1}{2},-\frac{1}{2}\right]_A}\right)\cos\left(\theta^{n_A}_{\left[0,\frac{1}{2},\frac{1}{2}\right]_A}\right)\right|, \quad u^A_{24}=\left|\cos\left(\theta^{n_A}_{\left[\frac{1}{2},-\frac{1}{2},0\right]_A}\right)\cos\left(\theta^{n_A}_{\left[-\frac{1}{2},\frac{1}{2},0\right]_A}\right)\right| \\
u^A_{25}&=\left|\cos\left(\theta^{n_A}_{\left[\frac{1}{2},0,-\frac{1}{2}\right]_A}\right)\cos\left(\theta^{n_A}_{\left[-\frac{1}{2},0,\frac{1}{2}\right]_A}\right)\right|, \quad u^A_{26}=\left|\cos\left(\theta^{n_A}_{\left[0,\frac{1}{2},-\frac{1}{2}\right]_A}\right)\cos\left(\theta^{n_A}_{\left[0,-\frac{1}{2},\frac{1}{2}\right]_A}\right)\right|
\end{aligned} \tag{30b}$$

and

$$u^\Lambda_{4J}=\sum_{I=1}^{6}u^\Lambda_{2J}u^\Lambda_{2I} \tag{30c}$$

3.5.2 FCC Crystal

For FCC crystal, the reciprocal vectors from the vectors that span its primitive cell form a BCC structure; which is a group of vector $\left\langle \frac{1}{2b}, \frac{1}{2b}, \frac{1}{2b} \right\rangle$ where the following 4 pairs satisfy (16):

$$\left[\frac{1}{2b}, \frac{1}{2b}, \frac{1}{2b}\right] \text{ and } \left[-\frac{1}{2b}, -\frac{1}{2b}, -\frac{1}{2b}\right], \qquad \left[\frac{1}{2b}, -\frac{1}{2b}, \frac{1}{2b}\right] \text{ and } \left[-\frac{1}{2b}, \frac{1}{2b}, -\frac{1}{2b}\right]$$
$$\left[-\frac{1}{2b}, \frac{1}{2b}, \frac{1}{2b}\right] \text{ and } \left[\frac{1}{2b}, -\frac{1}{2b}, -\frac{1}{2b}\right], \qquad \left[\frac{1}{2b}, \frac{1}{2b}, -\frac{1}{2b}\right] \text{ and } \left[-\frac{1}{2b}, -\frac{1}{2b}, \frac{1}{2b}\right] \quad (31)$$

4. Coefficients in Phase Field Model and Atomistic Computation

4.1 Surface Energy and Stacking Fault Energy

After applying (29-31) there are still two undetermined coefficients in (25): the reference density coefficient ρ_0 and an implicit length scale "*w*" that characterizes the thickness of interface surface layer between grains *B* and *A*. The latter determines the amplitude of the gradient $\nabla\eta$ on a boundary. These two coefficients can be calibrated if the amplitude of interface surface energy (27) is known for at least two cases in a one specie polycrystalline system.

The first case is that grain *A* and *B* have the same orientation but with misfit in atomic positions. The corresponding grain boundary is created by a shift of grain B in a direction tangential to the grain boundary surface, which can be considered as a stacking fault (incomplete edge dislocation) with the corresponding locally stored dislocation energy less or equal Peierls' energy barrier. When such a shift occurs over multiple atomic layers, according to (24) the upper bound of the accumulated energy per unit surface area is:

$$n_s \gamma_P = 2 n_s h_0 \quad (32)$$

where γ_P is the Peierls' energy barrier with the dimension of energy per unit area and n_s is the number of piled atomic layers with the stacking faults. The second case is that grain *B* vanishes, which can be considered as the extreme case that the grain boundary is formed by vacant sites with very large widthness, so such a grain boundary is identical to the free surface of grain *A* to vacuum with a surface energy γ_S. Once γ_S and γ_P are known, ρ_0 and "*w*" are fixed.

Many sophisticated considerations that bridge phase field model and atomistic computation can be found, e.g. [27, 32, 70-73]. This study suggests using the density function theory-based quantum computation [70, 72, 74] to compute γ_S and γ_P. Fig. 4a explains the process to compute γ_S: which is the difference in total energy between two states of the system: the equilibrium positions and that separated into two half of atomic slabs. This is because the work required to split the atomic supercell is the coherent energy E^{coh} that is transformed into the energy to form two new surfaces, i.e.

$$E^{coh} = 2\gamma_S \tag{33}$$

Figs. 4b,c show such a half atomic cell splitted along $[001]$ direction and the corresponding electron charge density $\rho(\boldsymbol{r})$ on (110) plane. Fig. 5 is the supercell to compute the slipping-induced dislocation along $[\bar{1}\,\bar{1}\,1]$ direction and the corresponding energy barrier. Examples of BCC iron and FCC Aluminum crystal are computed and the results are listed in table I.

Table I

	Fe(bcc) J/M^2	Al(fcc) J/M^2
$\gamma_S[001]\left(=\frac{E^{coh}_{[001]}}{2}\right)\approx$	2.715	0.93
$\gamma_P \approx$	0.49	0.17

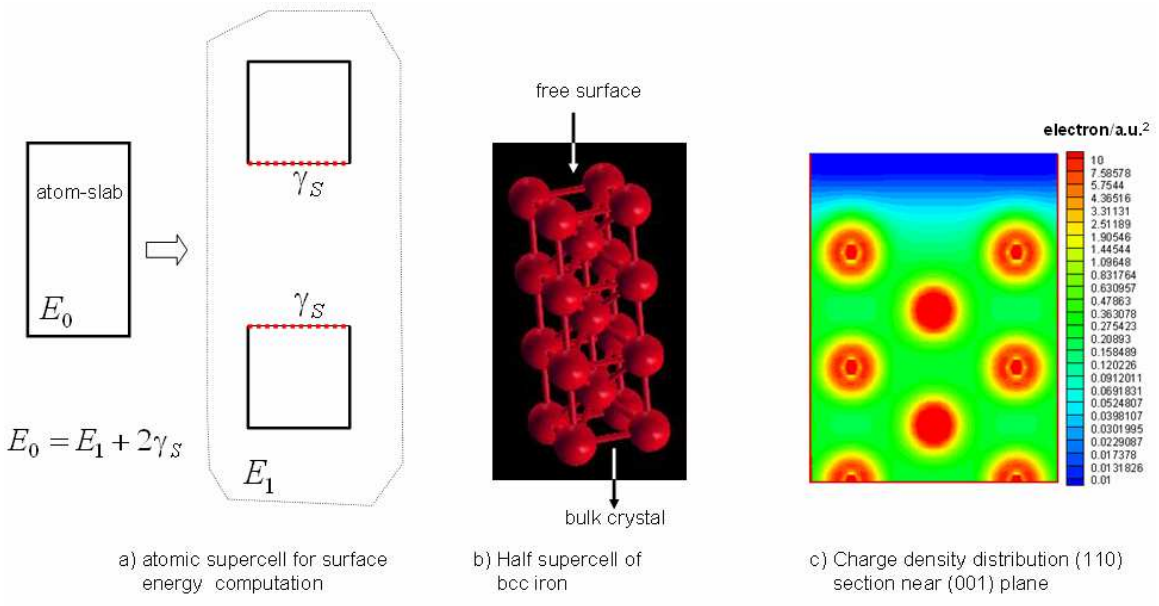

a) atomic supercell for surface energy computation

b) Half supercell of bcc iron

c) Charge density distribution (110) section near (001) plane

Fig.4 Computation of surface energy and charge density distribution near (001) free-surface of BCC iron

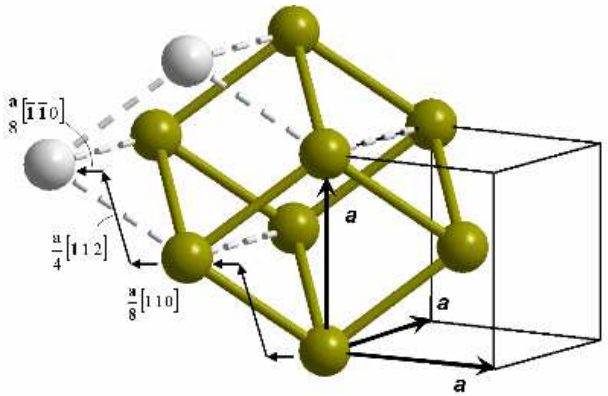

Fig. 5 Supercell used for computing Peierls' energy barrier in BCC crystal

By substituting obtained γ_S and γ_P into (27) and expanding η^Λ into Fourier series across the thickness of grain boundary layer *w*, under certain approximations the following relations are finally reached:

$$\rho_0 = \frac{\gamma_P}{bk_B T k_0}, \qquad w \approx \frac{k}{2}\frac{\gamma_S}{\gamma_P} b \tag{34}$$

where *b* is Burger's vector; *k*, k_0 are constants and *k* is about unit. It should be noticed that according to Fig. 3c the grain boundary width "*w*" in (34) is the interval where the order parameter $0 < \eta < 1$. It is much greater than the visible "grain boundary", denoted as w_o, which represents the significant disorder of atomic positions. Usually, $w_o \approx 0.3 - 0.5w$.

The derivation of (34) and detailed expressions of the constants are given by Appendix II.

5. Computer Implementation and Numerical Results

For single specie cubic polycrystalline system, by substituting (34) into (25) the latter becomes:

$$\Delta F = \kappa_F \int d\boldsymbol{x}^3 \left\{ f_0(\eta,\theta) + \kappa_S \Gamma\left(\nabla\eta, \nabla^2\eta, \theta, \psi\right)\right\} \tag{35}$$

and

$$\kappa_F = \frac{\gamma_P}{2bk_0}, \qquad \kappa_S = 2\pi^2 b^2 \tag{35a}$$

$$f_0(\eta,\theta) = \sum_{\Lambda=A,B}\sum_I \frac{u_{2I}^\Lambda}{\bar{u}_2^\Lambda}(2+a_I)\left(\eta^\Lambda\right)^2 + 4\sum_{\Lambda,\Lambda_1=A,B}\sum_I \frac{u_{2I}^\Lambda}{\bar{u}_2^\Lambda}\left(\eta^\Lambda\right)^2\left(\eta^{\Lambda_1}\right)^2 \tag{35b}$$

$$\Gamma\left(\eta,\nabla\eta,\nabla^2\eta,\theta,\psi\right) = \sum_{\Lambda=A,B}\sum_I \frac{u_{2I}^\Lambda}{\bar{u}_2^\Lambda} b_I\left[\left(\cos\theta_I^\Lambda\right)^2\left|\nabla\eta^\Lambda\right|^2 + \eta^\Lambda\left|\nabla\eta^\Lambda\right|\left|\nabla\theta_I^\Lambda\right|\right] \tag{35c}$$

$$\theta_I^{\Lambda} = \cos^{-1}\left(\frac{\boldsymbol{K}_I^{\Lambda}}{\left|\boldsymbol{K}_I^{\Lambda}\right|}\cdot \boldsymbol{n}_{\Lambda}\right) \tag{35d}$$

$$u_{2I}^{\Lambda} = \left|\cos\theta_{\boldsymbol{K}_I}^{\boldsymbol{n}_{\Lambda}}\cos\theta_{-\boldsymbol{K}_I}^{\boldsymbol{n}_{\Lambda}}\right| \qquad \text{defined by (29-31)}$$

$$\bar{u}_2^{\Lambda} = \sum_I u_{2I}^{\Lambda} \qquad \text{defined by (28)}$$

$$a_I = 1 - \frac{h_0}{h_p} - \sin^2\left(2\pi b\left|\boldsymbol{K}_I\right|\right) \qquad \text{defined by (24)}$$

$$b_I = \cos^2\left(2\pi b\left|\boldsymbol{K}_I\right|\right)$$

where b is Burger's vector; κ_F is a constant coefficient; h_0 and h_p are average Peierls' energy and height of the energy barrier, respectively; so $h_p = \gamma_P$; θ_I^{Λ} is the angles between surface normal $\boldsymbol{n}_{\Lambda}$ and reciprocal vector $\boldsymbol{K}_I^{\Lambda}$ in grain Λ; in cubic system $\boldsymbol{K}_I^{\Lambda}$ coincides one of crystal orientations of the grain. Thus, the functions $\sin\left(2\pi b\left|\boldsymbol{K}_I\right|\right)$, $\cos\left(2\pi b\left|\boldsymbol{K}_I\right|\right)$, and angles θ_I^{Λ} essentially represent the effects of grain boundary misorientation and tilt in phase field evolution.

Based on the analysis of [4, 7, 59] in the numerical simulation performed in this research the Ginzburg-Landau's kinetic has been applied:

$$\frac{\partial\eta}{\partial t} = -\frac{\partial\Delta F}{\partial\eta} - \kappa_s\sum_{\Lambda=A,B}\sum_I \frac{u_{2I}^{\Lambda}}{\bar{u}_2^{\Lambda}} b_I \eta^{\Lambda}\nabla^3\eta^{\Lambda}\cdot\left(\frac{\partial \boldsymbol{x}}{\partial\eta}\right) \tag{36}$$

where the subtraction of the second term on the right hand side ensures the evolution law (36) is within the framework of generalized diffusion equation, like, e.g. (2).

Following the idea developed in [59], the Ginzburg-Landau's kinetic for the evolution of surface angler is given by

$$\frac{\partial\theta_I^{\Lambda}}{\partial t} = -\varepsilon^2\frac{\partial\Delta F}{\partial\theta_I^{\Lambda}}, \qquad \varepsilon = \left\|\boldsymbol{Q}^{\Lambda\Lambda'} - \boldsymbol{I}\right\| \tag{37}$$

where Λ' denotes the grain Λ' adjacent to grain Λ; the norm of a second order tensor $\boldsymbol{A}$ is expressed as $\|\boldsymbol{A}\| = \sqrt{A_{11}^{\ 2} + A_{22}^{\ 2} + A_{33}^{\ 2}}$.

5.1 Anisotropic Case: Comparison with WKC Model

By comparing (40) with (3), the WKC model[10, 11, 59], one can find that (35) and (3) will coincide each other when the following relations hold:

$$f(\eta,T)_{eq.3} \to \kappa_F f(\eta,\theta)_{eq.35} \tag{38a}$$

and

$$\alpha^2\Gamma^2\left(|\nabla\eta|,\theta-\psi\right) = -\kappa_F\kappa_S \sum_{\Lambda=A,B}\sum_{I} \frac{u_{2I}^{\Lambda}}{\overline{u}_2^{\Lambda}} b_I \left(\cos\theta_I^{\Lambda}\right)^2 \left|\nabla\eta^{\Lambda}\right|^2 \tag{38b}$$

$$sg(\eta) = -\kappa_F\kappa_S \sum_{\Lambda=A,B}\sum_{I} \frac{u_{2I}^{\Lambda}}{\overline{u}_2^{\Lambda}} b_I \left[\eta^{\Lambda}\left|\nabla\eta^{\Lambda}\right|\nabla\theta_I^{\Lambda}\right], \qquad \frac{\varepsilon^2}{2} h(\eta) = 0 \tag{38c}$$

The term in the second relation of (38c) is introduced in [10, 11, 59] for the rotation between misfitted grains, which is taken care by kinetic relation (37) in this study.

5.2 Isotropic Case

Under this condition: $\cos\theta_I^{\Lambda} = 1$ and $u_{2I}^{\Lambda} = u_{2J}^{\Lambda}$ for any pair of $\{I,J\}$ in (35). Then by comparing (40) with (4), one can find that the following relations hold:

$$\alpha = -\frac{\gamma_P}{bk_0}(2+a_I), \quad \gamma = \frac{8\gamma_P}{bk_0}, \quad \beta = \gamma, \quad \kappa = \frac{2\gamma_P\pi^2 b b_I}{k_0} \tag{39}$$

However, the term $\eta^{\Lambda}\left|\nabla\eta^{\Lambda}\right|\left\|\nabla\theta_I^{\Lambda}\right|$ in (35) has no its counterpart in (4). $\left|\nabla\theta_I^{\Lambda}\right|$ is proportional to the inverse of grain boundary curvature and it usually is a higher order small quantity as compared with other terms.

5.3 Numerical Results

The Ginzburg-Landau expression of free energy (35) and the phase field kinetics (36, 37) have been implemented into a finite difference computer code. The experimental result of Naval Research Laboratory [75] provides a set of discretized data of a single specie polycrystalline system, which has been used as the initial condition for the grain coarsening simulation.

We first consider isotropic case, investigating the relationship between grain boundary thickness and the coefficients in the free energy (35). Fig. 6a shows examples of a single specie system by which a square grain contains a circle grain with two different pre-assigned grain boundary thicknesses (*w*). The square is discretized by 269x269 interpolating points with a uniform spacing "*h*" in-between. The model on left has the initial $w = 15h$ whereas on the one on right the initial $w = 4h$. Plotted in Fig. 6b are the evolutions of the boundary thicknesses, i.e. "*w*", for four different pre-assigned initial values with pre-assigned $\kappa_F = 1$ and $\kappa_S = 2$. As demonstrated by the figure, regardless initial value "*w*" approaches to the same value within the first 10 time increments for all four cases; which proves that the phase field formulation leads to stable grain boundary thickness during coarsening when its coefficients are fixed. In the computations demonstrated in this paper, the thickness "*w*" is defined as the width of the

strip within which the production of the order parameters η^A and η^B from two adjacent grains is less than 0.9, see Fig. 3c.

According to (35a) and (34):

$$\kappa_F \kappa_S = \frac{\pi^2}{k_0}\gamma_P b = \gamma_P k_w w \qquad k_w = \frac{2\pi^2}{k_0 k}\left(\frac{\gamma_P}{\gamma_S}\right) \tag{40}$$

On other hand, in (35) the product $\kappa_S \kappa_F$ scales the gradient term $\Gamma\left(\nabla\eta, \nabla^2\eta, ...\right)$. The second equality in the first relation of (40) indicates that this product coincides to the energy dissipation when a dislocation passes a distance " wk_w ". Hence, it can be anticipated that this product essentially controls the grain boundary thickness in the phase field model. In order to verify this prediction, plotted in Fig. 7a are the four computations of the two-grain system in Fig. 6 with the same initial thickness and fixed coefficients: $\gamma_P \cdot k_b = 1$, $\frac{\gamma_P}{\gamma_S} = 3$; but varying b = 0.5, 0.7, 1., 1.4. Different grain boundary thickness, "w", have been obtained after tens time steps. On contrast, Plotted in Fig. 7b are the results from the same examples in Fig. 7a but the computed grain boundary thickness has been normalized by the product of $\kappa_S \kappa_F$. As expected, they approach to the same value.

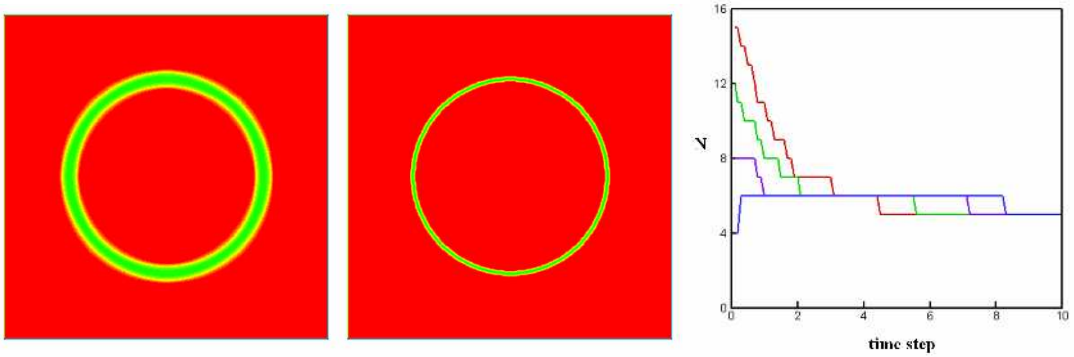

(a) (b)

Fig. 6 Bi-grain system for numerical test: (a) two assigned initial grain boundary thickness $w = Nh$ for $N = 15$ and $N = 4$, respectively; (b) changes of grain boundary thickness when time step increases; the four computations with different initial thicknesses converge into the same value. In these computations: $\kappa_F = 1$ and $\kappa_S = 2$ are taken.

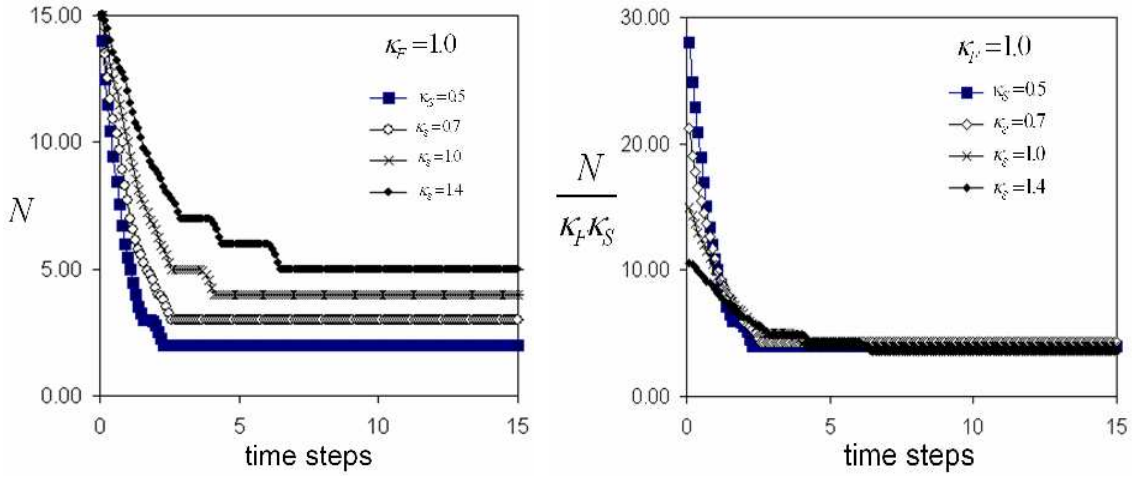

(a) (b)

Fig. 7 The relationship between the coefficients κ_F, κ_S and the computed grain boundary thickness $w = Nh$; where κ_F scales the amplitude of free energy in grain and the product $\kappa_S \kappa_F$ scales the energy associated with the gradient of order parameter.

Multiple two-dimensional computations of polycrystalline system have been carried out for three cases: (i) isotropic grains; (ii) two-dimensional grains with titled orientation; (iii) a two dimensional slice of three-dimensional grains with grain boundary title and misorientation. The results are plotted in Fig. 8. For the anisotropic cases the initial orientation of grains is assigned according the experimental results performed in Naval Research Laboratory[75], so in these figures the colors represent the angle between the y coordinate and $[010]$ direction for (ii) and (iii). These results demonstrate that the crystal anisotropy does bring up differences. A remarkable trend is that in the isotropic system (i) the grain growth is relatively "homogenous", since after a while of coarsening some small grains are still there whereas they disappear in other two cases. Also, in anisotropic system it seems that the propagation of low angle grain boundaries (the border between adjacent grains with similar colors) is faster than that of the high angle grain boundaries (the border between adjacent grains with higher contrast in colors); which results in larger individual grains. This could be a reason for the abnormal grains in experimental observations. The three dimensional computation in Fig. 9 is based on the initial condition of NRL experiment[75]. The example in Fig. 10 is computed by a random pre-assigned initial condition, which provides the view of the coarsening inside the polycrystalline.

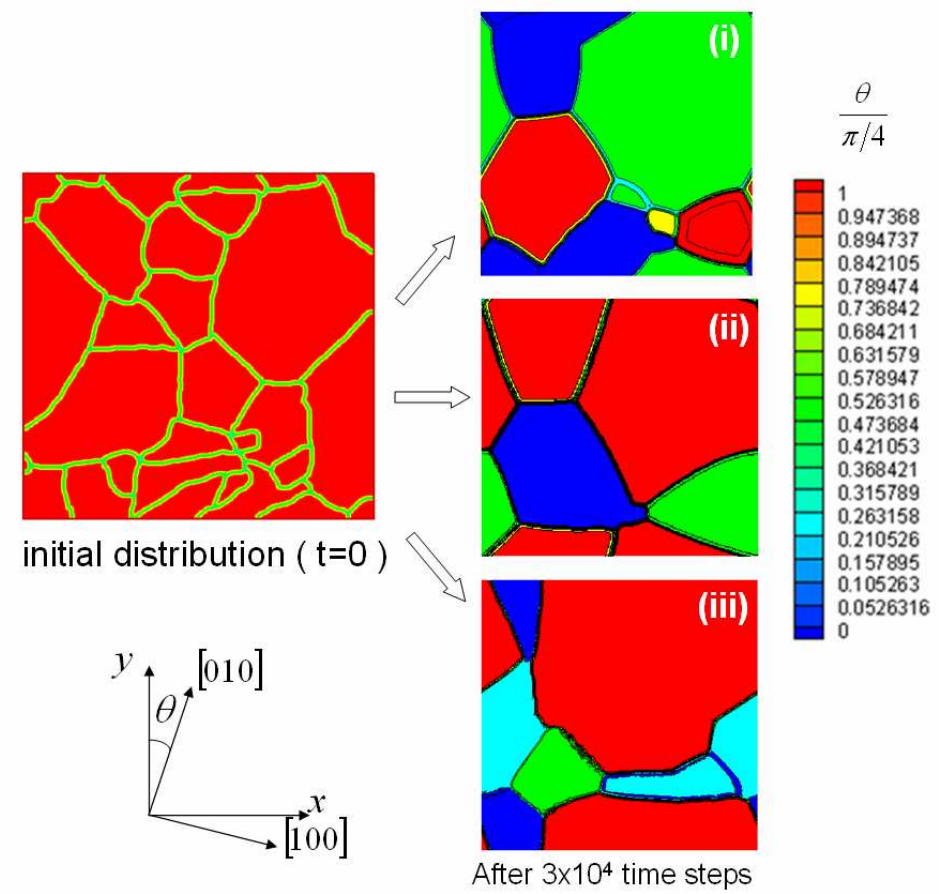

Fig. 8 Comparison of phase-field simulation based on (40) for (i) isotropic grains; (ii) grains with titled angles in 2D plane; (iii) a 2D slice of 3D grains with grain boundary title and misorientation. These results show a trend that isotropic approximation leads to relatively "homogenously" grain growth whereas abnormal-sized grains appear in anisotropic cases.

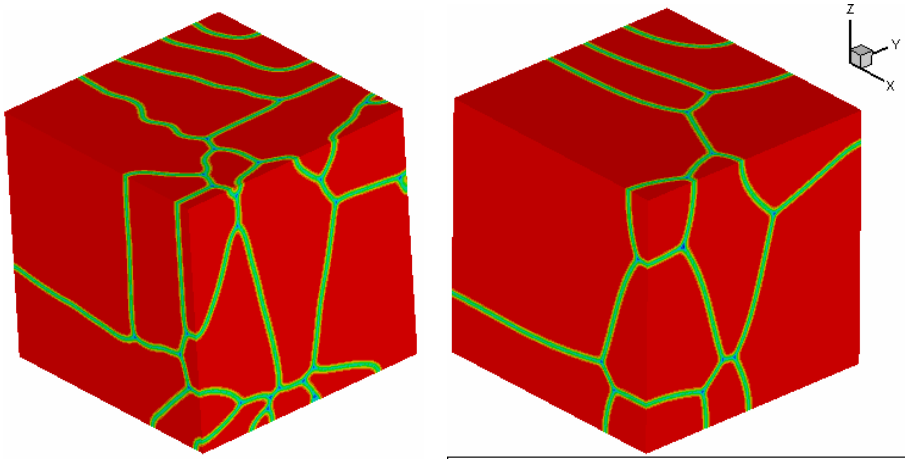

(a) time step = 100 (b) time step = 80000

Fig. 9 An example of 3D phase field simulation at two time steps; the NRL experimental result[75] is used to give initial grain sizes and distribution.

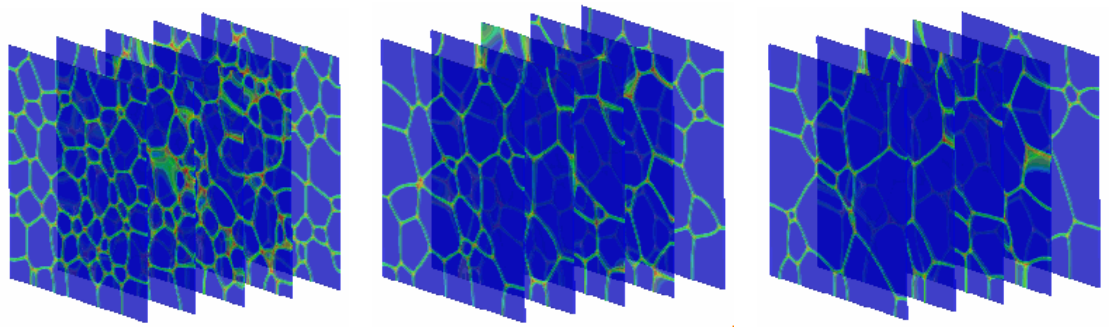

(a) initial (b) 15000 steps (c) 30000 steps

Fig. 10 Another 3D example with randomly initial condition; the polycrystalline slab is sliced into 5 sections to view inside the slab; the "thick" grain boundaries are those interface surfaces which are almost parallel to section.

6. Conclusions

A challenge in phase field modeling of grain coarsening is to establish the quantitative relationship between mathematic expression of free energy field and the complexities caused by grain boundary geometry, crystallography and the criteria to define associated energy measurements. In this study a "generalized dislocations zone" is proposed to model grain boundary while phase field order parameter is assigned as a scaling factor of electron gas density distributions in crystals. The difference in orientations between the two adjacent grains is considered in general as a superposition of a clockwise misorientation rotation, an anticlockwise title rotation, and a rotation of grain boundary surface. Ginzburg-Landau expansion has been applied to describe free energy and it fluctuation at grain boundary; in which the Peierls-Nabbaro's dislocation potential defines a "direct structure factor" that characterizes the order of atoms position in solid crystals. For coarsening process, this structure factor essentially governs the stiffness of grain boundary. Therefore, in the proposed phase field model of anisotropic grain coarsening, all coefficients in the free energy formulation can be determined through crystallography analysis and *Ab Initio* quantum mechanical computation or molecular dynamic simulation. In the proposed phase model the coefficients are fixed according to the amplitudes of stacking fault energy γ_P and surface energy γ_S

Analysis of BCC iron and FCC aluminum have been conducted, indicates the "theoretical" grain boundary thickness w to be approximately proportional to the product of Burger's vector "b" and the ratio $2\gamma_S/\gamma_P$. The product $2b\gamma_S/\gamma_P$ is the scaling parameter to the gradient part in the proposed phase field free energy. This "theoretical" thickness represents the interval where the order parameter neither vanishes nor be unit; hence it is usually about two to three time greater than visible grain boundaries thickness. The obtained conclusions have been verified by the numerical computations for a bicrystal system with different Burger's vector. The performed two- and three-dimensional polycrystalline computations demonstrate the proposed anisotripic formulation is applicable for large scale simulation. The developed phase field model can be considered as an extent of the combination of the achievements reported in [1-15].

Appendix I: Derivation of (21,22)

The relation (19), i.e. the secondary variation of (17), can be expressed as Ornstein-Zernike relation (see [36], eq.66):

$$\frac{\delta^2 F[\rho]}{\delta\rho(\boldsymbol{r})\delta\rho(\tilde{\boldsymbol{r}})} = k_B T\left[\frac{\delta(\boldsymbol{r}-\tilde{\boldsymbol{r}})}{\rho_0} - C(\rho_0;\boldsymbol{r}-\tilde{\boldsymbol{r}})\right] \tag{a1}$$

where $C(\rho_0;\boldsymbol{x}-\tilde{\boldsymbol{x}})$ is a direct correlation function to be determined, corresponding to an interface surface with an outer normal $\boldsymbol{n}$; ρ_0 is a constant coefficient in (10,11). The first term on the right hand of (a1) is relevant to the dilatation stiffness whereas the second term is correlated to shear modules. According to [32, 36], when $C(\rho_0;\boldsymbol{r}-\tilde{\boldsymbol{r}}) = C(\boldsymbol{r}-\tilde{\boldsymbol{r}})/\rho_0$, its Fourier transform, i.e.

$$\Im\left[\frac{C(\boldsymbol{r})}{\rho_0}\right] = \frac{\hat{C}[\boldsymbol{K}]}{\rho_0} = \frac{1}{\rho_0}\int_{\Omega} d\boldsymbol{r}^3 C(\boldsymbol{r}) exp(i\boldsymbol{K}\cdot\boldsymbol{r}) \tag{a2}$$

can be expanded into Taylor's series in the power of $\boldsymbol{K}^2$:

$$\begin{aligned}\hat{C}[\boldsymbol{K}] &= \hat{C}_0[\boldsymbol{K}] + \hat{C}_2[\boldsymbol{K}]\boldsymbol{K}^2 + \hat{C}_4[\boldsymbol{K}]\boldsymbol{K}^4 + ... \\ &= \alpha_0 + \alpha_2\boldsymbol{K}^2 + \alpha_4\boldsymbol{K}^4 + ...\end{aligned} \tag{a3}$$

Hence

$$\frac{\partial^2\hat{C}[\boldsymbol{K}]}{\partial\boldsymbol{K}^2} = 2\alpha_2 + 12\alpha_4\boldsymbol{K}^2 + ... \tag{a4}$$

so (a2) can be rewritten in the form as

$$\hat{C}[\boldsymbol{K}] = \alpha_0 + \frac{1}{2}\frac{\partial^2\hat{C}[\boldsymbol{K}]}{\partial\boldsymbol{K}^2}\boldsymbol{K}^2 - \frac{5}{24}\frac{\partial^4\hat{C}[\boldsymbol{K}]}{\partial\boldsymbol{K}^4}\boldsymbol{K}^4 + ... \tag{a5}$$

On other hand, by substituting (a1) into (19):

$$\Delta F_2 = \frac{k_B T}{2}\int_{\Omega}\int_{\Omega} d\boldsymbol{r}^3 d\tilde{\boldsymbol{r}}^3\left[\frac{\delta(\boldsymbol{r}-\tilde{\boldsymbol{r}})}{\rho_0} - C(\rho_0;\boldsymbol{r}-\tilde{\boldsymbol{r}})\right]\delta\rho(\boldsymbol{r})\delta\rho(\tilde{\boldsymbol{r}}) \tag{a6}$$

The coordinate $\boldsymbol{r}$ and $\hat{\boldsymbol{r}}$ can be related each other by $\hat{\boldsymbol{r}} = f(\boldsymbol{r})$ where $f(\boldsymbol{r})$ is an arbitrary one to one mapping, e.g. $f(\boldsymbol{r}) = -\boldsymbol{r}$. According to the derivation presented in [36]*, by applying Fourier transformation "$\Im$" to (a6) with convolution, it becomes:

$$\Im[\Delta F_2] = \frac{k_B T}{2} \int_{\Omega} d\tilde{\boldsymbol{r}}^3 \sum_{\boldsymbol{K},\tilde{\boldsymbol{K}}} \left[1 - \hat{C}(\boldsymbol{K})\right] \delta\hat{\rho}(\boldsymbol{K}) \delta\hat{\rho}(\tilde{\boldsymbol{K}}) \tag{a7}$$

where the upper hat denotes Fourier transformation and $\tilde{\boldsymbol{K}} = f(\boldsymbol{K})$.

For an arbitrary square-integrable function $q(\tilde{\boldsymbol{r}})$ in real space $\Re$ and $q(\tilde{\boldsymbol{r}})$ is with C_N continuity where $N \geq 2$, e.g., $q(\tilde{r}) = \delta\rho(\tilde{r})\delta\rho(f(\tilde{r}))$, the following relations hold:

$$q(\tilde{\boldsymbol{r}}) = \int_{\Omega_K} \hat{q}(\boldsymbol{K}) \exp(-i\boldsymbol{K} \cdot \tilde{\boldsymbol{r}}) d\boldsymbol{K} \tag{a8}$$

$$\nabla_{\tilde{r}} q(\tilde{\boldsymbol{r}}) = -i\boldsymbol{K} \int_{\Omega_K} \hat{q}(\boldsymbol{K}) \exp(-i\boldsymbol{K} \cdot \tilde{\boldsymbol{r}}) d\boldsymbol{K} \tag{a9}$$

$$\nabla_{\tilde{r}} \cdot \nabla_{\tilde{r}} q(\tilde{\boldsymbol{r}}) = -\boldsymbol{K} \cdot \boldsymbol{K} \int_{\Omega_K} \hat{q}(\boldsymbol{K}) \exp(-i\boldsymbol{K} \cdot \tilde{\boldsymbol{r}}) d\boldsymbol{K} \tag{a10}$$

On other hand, when $\tilde{\eta}_0(\boldsymbol{r}) = 0$ in (20) and $\tilde{\boldsymbol{r}} = f(\boldsymbol{r}) = -\boldsymbol{r}$, $\tilde{\boldsymbol{K}} = f(\boldsymbol{K})$, one has

$$\begin{aligned} \nabla_{\tilde{r}} \left[\delta\rho_K(\boldsymbol{r}) \delta\rho_K(f(\boldsymbol{r}))\right] = & \left\{\nabla_{\tilde{r}} \left[\eta_K(\boldsymbol{r}) \eta_K(f(\boldsymbol{r}))\right] + i(\boldsymbol{K} + f(\boldsymbol{K})) \eta_K(\boldsymbol{r}) \eta_K(f(\boldsymbol{r}))\right\} * \\ & \rho_0^2 \sum_{K, f(K)} u_K u_{f(K)} \exp(i(\boldsymbol{K} + f(\boldsymbol{K})) \cdot \boldsymbol{r}) \\ = & \nabla_{\tilde{r}} \left[\eta_K(\boldsymbol{r}) \eta_K(\tilde{\boldsymbol{r}})\right] \rho_0^2 \sum_{K,\tilde{K}} u_K u_{\tilde{K}} \delta_{0, K+\tilde{K}} \end{aligned} \tag{a11}$$

By substituting (a3) into (a7), performing inverse Fourier transformation and applying (a8-a11), after omitting the terms with the order of $\boldsymbol{K}$ higher than two the (a6) can be written in general:

$$\Delta F_2 \approx \frac{k_B T \rho_0}{2} \sum_{\boldsymbol{K},\tilde{\boldsymbol{K}}} u_{\tilde{K}} u_K \int_{\Omega} d\boldsymbol{r}^3 \left[(1 - \alpha_0) \eta_K(\boldsymbol{r}) \eta_{\tilde{K}}(\boldsymbol{r}) + \alpha_2 \nabla \cdot (\eta_K(\boldsymbol{r}) \nabla \eta_{\tilde{K}}(\boldsymbol{r}))\right] \tag{a12}$$

where the relation (16), hence $\eta_K(\tilde{\boldsymbol{r}}) = \eta_{\tilde{K}}(\boldsymbol{r})$, have been applied.

The (a12) can be rewritten in the following alternated expression:

---

* See page. 159 in [36], equation (67) and following analysis

$$\Delta F_2 \approx \frac{k_B T \rho_0}{2} \sum_{\boldsymbol{K},\tilde{\boldsymbol{K}}} u_{\tilde{\boldsymbol{K}}} u_{\boldsymbol{K}} \delta_{0,K+\tilde{\boldsymbol{K}}} \int_{\Omega} d\boldsymbol{r}^3 \left[\frac{\eta_K(\boldsymbol{r})\eta_{\tilde{K}}(\boldsymbol{r})}{S[\boldsymbol{K}]} + \frac{1}{2} \frac{\partial^2 \hat{C}[\boldsymbol{K}]}{\partial \boldsymbol{K}^2} \frac{\boldsymbol{K}^2}{|\boldsymbol{K}|^2} : \left(\nabla\left(\eta_K(\boldsymbol{r})\nabla\eta_{\tilde{K}}(\boldsymbol{r})\right)\right) \right] \quad (21)$$

where the structure factor $S(\boldsymbol{K})$ is defined by

$$S(\boldsymbol{K}) = \left[1 - \hat{C}_0[\boldsymbol{K}]\right]^{-1} \quad (22)$$

Appendix II

Noticing that the gradient $\nabla\eta^{\Lambda}$ is perpendicular to grain boundary so $\nabla\eta^{\Lambda} = \boldsymbol{n}|\nabla\eta^{\Lambda}|$ where $\boldsymbol{n}$ is grain boundary normal. As illustrated in Fig. 3c, η^{Λ} varies from 1 to 0 which defines a grain boundary, so one may define a coordinate r varies from 0 to w to cross over the boundary layer accordingly. Then, η^{Λ} can be expanded into Fourier series across the thickness of grain boundary layer:

$$\eta^{\Lambda}(r) = \frac{1}{2}\left[\eta_0^{\Lambda} + \sum_{n=1}^{\infty} \eta_n^{\Lambda} \cos\left(\frac{n\pi r}{w}\right)\right] \qquad \text{for } r \in [0, w] \quad (b1)$$

with

$$\eta^{A}(0) = 1, \qquad \eta^{A}(w) = 0, \qquad \eta^{B}(0) = 0, \qquad \eta^{B}(w) = 1$$

Substituting (b1) into (27), then applying the condition (32) one obtains:

$$k_s \gamma_P = \frac{\rho_0 k_B T w}{2} \int_0^1 d\left(\frac{\boldsymbol{r}}{w}\right) \left\{ \begin{array}{l} 2\sum_{\Lambda=A,B} \left(\eta^{\Lambda}\right)^2 + \sum_{\Lambda,\Lambda_1=A,B} 4\left(\eta^{\Lambda}\right)^2 \left(\eta^{\Lambda_1}\right)^2 + \\ \sum_{\Lambda=A,B} \sum_{I} u_I \left[a_I \left(\eta^{\Lambda}\right)^2 + b_I \left(\left(\cos\theta_I^{\Lambda}\right)^2 \left|\nabla\eta^{\Lambda}\right|^2 + \eta^{\Lambda} \left|\nabla^2 \eta^{\Lambda}\right| \right) \right] \end{array} \right\} \quad (b2)$$

When the grain boundary outer normal $\boldsymbol{n}$ coincides $[001]$ and (24a) applies:

$$w = k_s b \quad (b3)$$

$$cos\,\theta_I^{\Lambda} = 1 \quad (b4)$$

$$a_I = 1 - E_0 = \frac{1}{2}, \qquad b_I = 2\pi^2 b^2 E_p = 2\pi^2 b^2 \quad (b5)$$

In (b3) b is Burger vector and k_s is a constant. Substituting (b3,b4,b5) into (b2) and performing the integral over the interval $[0, w]$, we finally obtain:

$$k_s \gamma_P = \rho_0 k_B T k_s b k_0 \quad (b6)$$

where

$$k_0 = \frac{1}{2}\int_0^w d\left(\frac{\boldsymbol{r}}{w}\right)\left\{\begin{array}{l} 2\sum_{\Lambda=A,B}\left(\eta^{\Lambda}\right)^2 + \sum_{\Lambda,\Lambda_1=A,B} 4\left(\eta^{\Lambda}\right)^2\left(\eta^{\Lambda_1}\right)^2 + \\ \sum_{\Lambda=A,B}\left[\left(\eta^{\Lambda}\right)^2 + 2\pi^2 b^2\left(\left|\nabla\eta^{\Lambda}\right|^2 + \eta^{\Lambda}\left|\nabla^2\eta^{\Lambda}\right|\right)\right] \end{array}\right\} \tag{b7}$$

Hence

$$\rho_0 = \frac{\gamma_P}{bk_B T k_0} \tag{b8}$$

The second case is free surface. Under this condition the grain *B* vanishes and the left hand side of (34) becomes γ_S. Assuming that the thickness *w* is the same as that in (b8):

$$\gamma_S = \rho_0 k_B T k_s b k_1 \tag{b9}$$

where

$$k_1 = \frac{1}{2}\int_0^w d\left(\frac{\boldsymbol{r}}{w}\right)\left\{\begin{array}{l} 2\left(\eta^{A}\right)^2 + 4\left(\eta^{A}\right)^4 + \\ \left[\left(\eta^{A}\right)^2 + 2\pi^2 b^2\left(\left|\nabla\eta^{A}\right|^2 + \eta^{A}\left|\nabla^2\eta^{A}\right|\right)\right] \end{array}\right\} \tag{b10}$$

Omitting tedious calculation, we finally obtain

$$\frac{w}{b} = k\frac{\gamma_S}{\gamma_P} \qquad \text{where} \qquad k = \frac{k_0}{k_1} \tag{b11}$$

For the grain boundaries with the heterogeneities illustrated in Fig. 2, by applying (5a-5d) and (32a) an alternative form of (39) is

$$\frac{w}{b} \approx \frac{k}{2}\frac{E^{GB}}{\gamma_P^{GB}} \approx \frac{E^{GB}}{\gamma_P^{GB}} \tag{b12}$$

So all coefficients of (25) are fixed and the scaling function η^{Λ}, i.e. the order parameter, is to be determined by phase field solution.

By omitting the terms for $n \geq 2$ in (b1), the coefficient on the right hand side of (b12) becomes

$$k \approx \frac{4.25 + 0.25 * \pi^4 \left(\frac{b}{w}\right)^2}{2.03 + 0.125 * \pi^4 \left(\frac{b}{w}\right)^2}$$

Substituting this relation into the first equality of (b12), one finds:

$$\frac{w}{b} \approx 2\frac{\gamma_S}{\gamma_P} = \frac{E^{GB}}{\gamma_P^{GB}} \tag{b13}$$

Substituting (b13) into (35a), one obtains the alternative expressions of the coefficients as following

$$\kappa_F = \frac{\gamma_S}{wk_0}\ , \qquad \kappa_S = \left(\frac{\gamma_P \pi}{\gamma_S}\right)^2 \frac{w^2}{2} \tag{b14}$$

and

$$\kappa_S \kappa_F = \gamma_P (w k_w) \qquad \text{or} \qquad \kappa_S \kappa_F = b(\gamma_P k_b) \tag{b15}$$

where

$$k_w = \frac{E_p \pi^2}{2k_0}\left(\frac{\gamma_P}{\gamma_S}\right) \qquad \text{and} \qquad k_b = \frac{\pi^2 E_p}{k_0} \tag{b16}$$

Acknowledgements. The results of isotropic two and three dimensional phase field model presented in this paper were partially sponsored by the Naval D3D project. The author would like to express his sincere gratitude to US Office of Naval Research and Dr. Christodoulou, project officer, for the support and many kind discussions. The author would also like to thank Professor Peter Voorhees, Department of Materials Science and Engineering, Northwestern University, for his many kind suggestions and advices during the researches presented in this paper.

References

1. Allen, S.M. and J.W. Cahn, *Microscopic Theory for Antiphase Boundary Motion and Its Application to Antiphase Domain Coarsening.* Acta Metallurgica, 1979. **27**(6): p. 1085-1095.

2. Cahn, J.W. and J.E. Hilliard, *Free Energy of a Nonuniform System .3. Nucleation in a 2-Component Incompressible Fluid.* Journal of Chemical Physics, 1959. **31**(3): p. 688-699.
3. Allen, S.M. and J.W. Cahn, *Ground State Structures in Ordered Binary-Alloys with Second Neighbor Interactions.* Acta Metallurgica, 1972. **20**(3): p. 423-&.
4. Warren, J.A., *How Does a Metal Freeze - a Phase-Field Model of Alloy Solidification.* Ieee Computational Science & Engineering, 1995. **2**(2): p. 38-49.
5. Chen, L.Q. and A.G. Khachaturyan, *Computer-Simulation of Decomposition Reactions Accompanied by a Congruent Ordering of the 2Nd Kind.* Scripta Metallurgica Et Materialia, 1991. **25**(1): p. 61-66.
6. Eggleston, J.J., G.B. McFadden, and P.W. Voorhees, *A phase-field model for highly anisotropic interfacial energy.* Physica D, 2001. **150**(1-2): p. 91-103.
7. Fan, D. and L.Q. Chen, *Computer simulation of grain growth using a continuum field model.* Acta Materialia, 1997. **45**(2): p. 611-622.
8. Karma, A., *Phase-Field Model of Eutectic Growth.* Physical Review E, 1994. **49**(3): p. 2245-2250.
9. Karma, A. and W.J. Rappel, *Quantitative phase-field modeling of dendritic growth in two and three dimensions.* Physical Review E, 1998. **57**(4): p. 4323-4349.
10. Kobayashi, R., J.A. Warren, and W.C. Carter, *Vector-valued phase field model for crystallization and grain boundary formation.* Physica D, 1998. **119**(3-4): p. 415-423.
11. Warren, J.A., Kobayashi, R., Lobovsky, A. E. and Carter, W. C., *Extending phase field models of solidification to polycrystalline materials.* Acta Materialia, 2003. **51**(20): p. 6035-6058.
12. Elder, K.R., Drolet, F., Kosterlitz, J. M., Grant, M., *Stochastic Eutectic Growth.* Physical Review Letters, 1994. **72**(5): p. 677-680.
13. Beckermann, C., Diepers, H. -J., Steinbach, I., Karma, A., Tong, X., *Modeling Melt Convection in Phase-Field Simulations of Solidification.* Journal of Computational Physics, 1999. **154**: p. 468-496.
14. Boettinger, W.J., Warren, J.A., Beckermann, C., Karma, A., *Phase-field simulation of solidification.* Annual Review of Materials Research, 2002. **32**: p. 163-194.
15. Haxhimali, T., Karma, A., Gonzales, F., Rappaz, M., *Orientation selection in dendritic evolution.* Nature Materials, 2006. **5**(8): p. 660-664.
16. Allen, S.M. and J.W. Cahn, *Coherent and Incoherent Equilibria in Iron-Rich Iron-Aluminum Alloys.* Acta Metallurgica, 1975. **23**(9): p. 1017-1026.
17. Cahn, J.W. and J.E. Hilliard, *Free Energy of a Nonuniform System .1. Interfacial Free Energy.* Journal of Chemical Physics, 1958. **28**(2): p. 258-267.
18. Cahn, J.W. and J.E. Hilliard, *On the Equilibrium Segregation at a Grain Boundary.* Acta Metallurgica, 1959. **7**(3): p. 219-221.
19. Karma, A. and W.J. Rappel, *Phase-field method for computationally efficient modeling of solidification with arbitrary interface kinetics.* Physical Review E, 1996. **53**(4): p. R3017-R3020.
20. Karma, A. and W.J. Rappel, *Numerical simulation of three-dimensional dendritic growth.* Physical Review Letters, 1996. **77**(19): p. 4050-4053.

21. Elder, K.R., Grant, M., Provatas, N., Kosterlitz, J. M., *Sharp interface limits of phase-field models.* Physical Review E, 2001. **6402**(2): Art. No. 021604.
22. Elder, K.R., Katakowski, M., Haataja, M., *Modeling elasticity in crystal growth.* Physical Review Letters, 2002. **88**(24): Art. No. 245701.
23. Warren, J.A. and W.J. Boettinger, *Prediction of Dendritic Growth and Microsegregation Patterns in a Binary Alloy Using the Phase-Field Method.* Acta Metallurgica Et Materialia, 1995. **43**(2): p. 689-703.
24. Elder, K.R. and M. Grant, *Modeling elastic and plastic deformations in nonequilibrium processing using phase field crystals.* Physical Review E, 2004. **70**(5): Art. No. 051605.
25. Greenwood, M., M. Haataja, and N. Provatas, *Crossover scaling of wavelength selection in directional solidification of binary alloys.* Physical Review Letters, 2004. **93**(24): Art. No. 246101.
26. Stefanovic, P., M. Haataja, and N. Provatas, *Phase-field crystals with elastic interactions.* Physical Review Letters, 2006. **96**(22), Art. No.225504.
27. Asta, M., Morgan, D., Hoyt, J. J., Sadigh, B., Althoff, J. D., de Fontaine, D., Foiles, S. M., *Embedded-atom-method study of structural, thermodynamic, and atomic-transport properties of liquid Ni-Al alloys.* Physical Review B, 1999. **59**(22): p. 14271-14281.
28. Asta, M., J.J. Hoyt, and A. Karma, *Calculation of alloy solid-liquid interfacial free energies from atomic-scale simulations.* Physical Review B, 2002. **66**(10): Art. No.100101.
29. Hoyt, J.J., M. Asta, and A. Karma, *Atomistic simulation methods for computing the kinetic coefficient in solid-liquid systems.* Interface Science, 2002. **10**(2-3): p. 181-189.
30. Upmanyu, M., et al., *Simultaneous grain boundary migration and grain rotation.* Acta Materialia, 2006. **54**(7): p. 1707-1719.
31. Hoyt, J.J., M. Asta, and A. Karma, *Atomistic and continuum modeling of dendritic solidification.* Materials Science & Engineering R-Reports, 2003. **41**(6): p. 121-163.
32. Wu, K.A., et al., *Ginzburg-Landau theory of crystalline anisotropy for bcc-liquid interfaces.* Physical Review B, 2006. **73**(9): p. -.
33. Jin, Y.M.M. and A.G. Khachaturyan, *Atomic density function theory and modeling of microstructure evolution at the atomic scale.* Journal of Applied Physics, 2006. **100**(1): p. -.
34. Alexander, S., Mctague, J., *Should All Crystals Be Bcc - Landau Theory of Solidfication and Crystal Nucleation.* Physical Review Letters, 1978. **41**(10): p. 702-705.
35. Ebner, C., Saam, W. F., Stroud, D., *Density-Functional Theory of Simple Classical Fluids. I. Surface.* Physical Review, A, 1976. **14**(6): p. 2264-2273.
36. Evans, R., *The Nature of the Liquid-Vapour Interface and Other Topics in the Statistical Mechanics of Non-Uniform, Classical Fluids.* Advances in Physics, 1979. **28**(2): p. 143-200.
37. Shih, W.H., et al., *Ginzburg-Landau Theory for the Solid-Liquid Interface of Bcc Elements.* Physical Review A, 1987. **35**(6): p. 2611-2618.

38. Khachaturyan, A.G., *Long-range order parameter in field model of solidification.* Philosophical Magazine a-Physics of Condensed Matter Structure Defects and Mechanical Properties, 1996. **74**(1): p. 3-14.
39. Wang, Y.U., Y.M.M. Jin, and A.G. Khachaturyan, *Mesoscale modelling of mobile crystal defects - dislocations, cracks and surface roughening: phase tield microelasticity approach.* Philosophical Magazine, 2005. **85**(2-3): p. 261-277.
40. Karma, A. and A.E. Lobkovsky, *Unsteady crack motion and branching in a phase-field model of brittle fracture.* Physical Review Letters, 2004. **92**(24): p. -.
41. Guyer, J.E., Boettinger, W. J., Warren, J. A., McFadden, G. B., *Phase field modeling of electrochemistry. I. Equilibrium.* Physical Review E, 2004. **69**(2): p. 021603.
42. Guyer, J.E., Boettinger, W. J., Warren, J. A., McFadden, G. B., *Phase field modeling of electrochemistry. II. Kinetics.* Physical Review E, 2004. **69**(2): p. 691064.
43. Ottino, J.M., *Complex systems.* Aiche Journal, 2003. **49**(2): p. 292-299.
44. Olson, G.B., *Computational design of hierarchically structured materials.* Science, 1997. **277**(5330): p. 1237-1242.
45. Oden, J.T., et al., *Research directions in computational mechanics.* Computer Methods in Applied Mechanics and Engineering, 2003. **192**(7-8): p. 913-922.
46. Belytschko, T., Liu, W.K., and Moran, B., *Nonlinear Finite Elements for Continua and Structures*. 2000, New York: John Wiley & Sons.
47. Hughes, T.J.R., L.P. Franca, and M. Mallet, *A New Finite-Element Formulation for Computational Fluid-Dynamics .1. Symmetrical Forms of the Compressible Euler and Navier-Stokes Equations and the 2nd Law of Thermodynamics.* Computer Methods in Applied Mechanics and Engineering, 1986. **54**(2): p. 223-234.
48. Voorhees, P.W. and M.E. Glicksman, *Analysis of Multiparticle Diffusion.* Journal of Metals, 1982. **35**(12): p. A84-A84.
49. Voorhees, P.W. and M.E. Glicksman, *Solution to the Multi-Particle Diffusion Problem with Applications to Ostwald Ripening .1. Theory.* Acta Metallurgica, 1984. **32**(11): p. 2001-2011.
50. Khachaturyan, A.G., *Theory of Structural Transformation in Solids*. 1976, New York: John Wiley & Sons.
51. Needleman, A., *Computational Mechanics at the Mesoscale.* Acta Materialia, 2000. **48**: p. 105-117.
52. Babuska, I. and J.T. Oden, *The reliability of computer predictions: Can they be trusted?* International Journal of Numerical Analysis and Modeling, 2006. **3**(3): p. 255-272.
53. Hughes, T.J.R. and J.R. Stewart, *A space-time formulation for multiscale phenomena.* Journal of Computational and Applied Mathematics, 1996. **74**(1-2): p. 217-229.
54. Frary, M., Schuh, C. A., *Grain Boundary Networks: Scaling Laws, Preferred Cluster Structure, and Their Implications for Grain Boundary Engineering.* Acta Materialia, 2005. **53**(16): p. 4323-4335.

55. Schuh, C.A., Kumar, M., King, W. E., *Analysis of Grain Boundary Networks and Their Evoluation during Grain Boundary Engineering.* Acta Materialia, 2003. **51**(3): p. 687-700.
56. Voorhees, P.W., Coriell, S. R., Mcfadden, G. R., Sekerka, R. F., *The Effect of Anisotropic Crystal Melt Surface-Tension on Grain-Boundary Groove Morphology.* Journal of Crystal Growth, 1984. **67**(3): p. 425-440.
57. Thornton, K., N. Akaiwa, and P.W. Voorhees, *Large-scale simulations of Ostwald ripening in elastically stressed solids: I. Development of microstructure.* Acta Materialia, 2004. **52**(5): p. 1353-1364.
58. Thornton, K., N. Akaiwa, and P.W. Voorhees, *Large-scale simulations of Ostwald ripening in elastically stressed solids. II. Coarsening kinetics and particle size distribution.* Acta Materialia, 2004. **52**(5): p. 1365-1378.
59. Kobayashi, R., J.A. Warren, and W.C. Carter, *A continuum model of grain boundaries.* Physica D-Nonlinear Phenomena, 2000. **140**(1-2): p. 141-150.
60. Chen, L.Q. and J. Shen, *Applications of semi-implicit Fourier-spectral method to phase field equations.* Computer Physics Communications, 1998. **108**(2-3): p. 147-158.
61. Fan, D.N., Chen, L. Q., Chen, S. P., Voorhees, P. W., *Phase field formulations for modeling the Ostwald ripening in two-phase systems.* Computational Materials Science, 1998. **9**(3-4): p. 329-336.
62. Hao, S., Hong, L., Binomiemi, R., Combs, D. M. G., Fett, G., *A Multi-Scale Model of Intergranular Fracture and Computer Simulation of Fracture Toughness of a Carburized Steel*. in *Int. Conf. on New Developments in Long and Forged Products*. 2006. Winter Park, Colorado, U. S. A.
63. Weertman, J., *Dislocation Based Fracture Mechanics*. 1996, London: World Scientific.
64. Weertman J. and Weertman, J. R., *Elementary Dislocation Theory* 1964, New York: Macmillan.
65. Rice, J.R., *Dislocation Nucleation from a Crack Tip - an Analysis Based on the Peierls Concept.* Journal of the Mechanics and Physics of Solids, 1992. **40**(2): p. 239-271.
66. Appel, F., Beaven, P. A., Wagner, R., *Deformation Processes Related to Interfacial Boundaries in 2-Phase Gamma-Titanium Aluminides,* Acta Metall. Maters., 1993, **41** (6): p. 1721-1732.
67. Appel, F., Wagner, R., *Microstructure and deformation of two-phase gamma-titanium aluminides*, MATERIALS SCIENCE & ENGINEERING R-REPORTS, 1998, **22** (5), p. 187-268.
68. Kohn, W., Sham, L. J., *Self-Consistent Equations Including Exchange and Correlation Effects.* Physical Review, 1965. **140**(4A): p. 1133-1138.
69. Hohenberg, P., Kohn, W, *Inhomogeneous Electron Gas.* Physical Review, 1964. **136**(3B): p. 864-871
70. Wimmer, E., Krakauer, H., Weinert, M., Freeman, A. J., *Full-Potential Self-Consistent Linearized-Augmented-Plane-Wave Method for Calculating the Electronic-Structure of Molecules and Surfaces - O2 Molecule.* Physical Review B, 1981. **24**(2): p. 864-875.

71. Asta, M.N., Ozolins, V., Hoyt, J. J., van Schilfgaarde, M., *Ab initio molecular-dynamics study of highly nonideal structural and thermodynamic properties of liquid Ni-Al alloys.* Physical Review B, 2001. **6402**(2), Art. No. 020201.
72. Mehl, M.J., Papaconstantopoulos, D. A., *Applications of a tight-binding total-energy method for transition and noble metals: Elastic constants, vacancies, and surfaces of monatomic metals.* Physical Review B, 1996. **54**(7): p. 4519-4530.
73. Hoyt, J.J. and M. Asta, *Atomistic computation of liquid diffusivity, solid-liquid interfacial free energy, and kinetic coefficient in Au and Ag.* Physical Review B, 2002. **65**(21): Art. No. 214106.
74. Krakauer, H. and A.J. Freeman, *Linearized Augmented Plane-Wave Method for the Electronic Band-Structure of Thin-Films.* Physical Review B, 1979. **19**(4): p. 1706-1719.
75. Lewis, A., Sponor, G., *D3D project review meeting, OSU, Oct,2005*. 2005.
76. Haasen, P., *Physical Metallurgy*, 1984. Cambridge University Press, Cambridge.
77. Freund, B., *Mechanics of Adhesion Contact*, A Presentation at Northwestern University, Evanston, June, 8th, 2007
78. Mataga, P.A., Freund, L. B., Hutchinson, J. W., *Crack Tip Plasticity in Dynamic Fracture.* J. Phys. Chem. Solids, 1987. **48**(11): p. 985-1005.
79. Hill, R., *Mathematical Theory of Plasticity*. 1951, Cambridge: Cambridge Express.